Semi-Annual Report Submitted to the
National Aeronautics and Space Administration

For July - December, 1996

Contract Number: NAS5-31370

Land Surface Temperature Measurements from EOS MODIS Data

MODIS Team Member
PRINCIPAL INVESTIGATOR

ZHENGMING WAN

P.I.'s Address:

ZHENGMING WAN
Institute for Computational Earth System Science
University of California
Santa Barbara, CA 93106-3060

phone : (805) 893-4541
Fax no: (805) 893-2578
Internet: wan@icess.ucsb.edu

Land Surface Temperature Measurements from EOS MODIS Data

Semi-Annual Report
For July - December, 1996

Zhengming Wan

Contract Number: NAS5-31370

Abstract

We have developed a physics-based land-surface temperature (LST) algorithm for simultaneously retrieving surface band-averaged emissivities and temperatures from day/night pairs of MODIS (Moderate Resolution Imaging Spectroradiometer) data in seven thermal infrared bands. The set of 14 nonlinear equations in the algorithm is solved with the statistical regression method and the least-squares fit method. This new LST algorithm was tested with simulated MODIS data for 80 sets of band-averaged emissivities calculated from published spectral data of terrestrial materials in wide ranges of atmospheric and surface temperature conditions. Comprehensive sensitivity and error analysis has been made to evaluate the performance of the new LST algorithm and its dependence on variations in surface emissivity and temperature, upon atmospheric conditions, as well as the noise-equivalent temperature difference (NEΔT) and calibration accuracy specifications of the MODIS instrument. In cases with a systematic calibration error of 0.5%, the standard deviations of errors in retrieved surface daytime and nighttime temperatures fall between 0.4-0.5 °K over a wide range of surface temperatures for mid-latitude summer conditions. The standard deviations of errors in retrieved emissivities in bands 31 and 32 (in the 10-12.5 μm IR spectral window region) are 0.009, and the maximum error in retrieved LST values falls between 2-3 °K. Several issues related to the day/night LST algorithm (uncertainties in the day/night registration and in surface emissivity changes caused by dew occurrence, and the cloud cover) have been investigated. The LST algorithms have been validated with MODIS Airborne Simulator (MAS) dada and ground-based measurement data in two field campaigns conducted in Railroad Valley playa, NV in 1995 and 1996. The MODIS LST version 1 software has been delivered.

1. INTRODUCTION

Land-surface temperature (LST) is one of the key parameters in the physics of land-surface processes on regional and global scales, combining the results of all surface-atmosphere interactions and energy fluxes between the atmosphere and the ground [Mannstein, 1987; Sellers et al., 1988]. Therefore it is required for a wide variety of climatic, hydrological, ecological and biogeochemical studies [Schmugge and André, 1991; Running et al., 1994]. In order to understand the Earth system better on the global scale, the Earth Observing System (EOS) will provide surface kinetic temperatures at specified accuracies of 0.3 °K for oceans and 1 °K for land. The international Tropical Ocean Global Atmosphere (TOGA) program has specified that sea surface temperature (SST) should be accurate to 0.3 °K for global numerical models of climate.

During the past decade, significant progress has been made in estimation of land-surface emissivity and temperature from airborne thermal infrared data. Kahle et al. [1980] developed a technique to estimate the surface temperature based on an assumed constant emissivity in one channel and previously determined atmospheric parameters. This temperature was then used to estimate the emissivity in other channels [Kahle, 1986]. Other techniques, such as thermal log residuals and alpha residuals, have been recently developed to extract emissivity information from multispectral thermal infrared data [Hook et al., 1992].

A variety of split-window methods have been developed to retrieve sea-surface temperature and land-surface temperature from NOAA AVHRR data. The split-window LST method corrects the atmospheric effects based on the differential absorption in adjacent infrared bands [Price, 1984; Becker, 1987; Wan and Dozier, 1989; Becker and Li, 1990; Sobrino et al., 1991; Vital, 1991; Kerr et al., 1992; Ottle and Stoll, 1993; Prata, 1994; Wan and Dozier, 1996]. A major problem in using split-window LST methods is that we need to know the surface emissivities in the bands better than 0.01. It seems possible to have such knowledge of the emissivities for certain types of land covers, such as lake surfaces, snow/ice, dense evergreen canopies, and some soils. For land covers with variable emissivities, especially in semi arid and arid areas, it is almost impossible to estimate two band-averaged emissivities to such accuracy. Therefore, it is necessary to develop new algorithms to retrieve LST without prior knowledge of surface emissivities. In addition, surface emissivity is also needed both to calculate up-welling thermal infrared radiation, and for environmental monitoring and geological mapping [Kahle, 1980].

Li and Becker [1993] proposed a method to estimate both land-surface emissivity and LST using pairs of day/night co-registered AVHRR images. They used a temperature-independent spectral index (TISI) in thermal infrared bands and assumed knowledge of surface TIR BRDF (thermal infrared Bidirectional Reflectance Distribution Function) and atmospheric profiles. Such combined a priori knowledge and information are not readily available in most situations. Wan and Li [1996] developed a MODIS day/night LST method that uses day/night pairs of TIR data in seven MODIS bands for simultaneously retrieving surface temperatures and band-averaged emissivities without knowing atmospheric temperature and water vapor profiles to high accuracy.

MODIS is an EOS instrument that will serve as the keystone [Salomonson et al., 1989] for global studies of atmosphere [King et al., 1992], land [Running et al., 1994], and ocean processes. It scans ±55° from nadir in 36 bands, with bands 1-19 and band 26 in the visible and near infrared range, and the remaining bands in the thermal infrared from 3 to 15 μm. The specifications of MODIS bands are shown in Table I. Figure 1 shows the total transmission and transmission functions corresponding to water vapor (H_2O) band absorption and continuum absorption, uniformly mixed gases (labeled by CO_2) and ozone absorptions. These transmission calculations were done for a typical scenario, using an updated atmospheric radiative transfer model, MODTRAN3 [Berk et al., 1989], the specific conditions are mid-latitude summer, clear-sky (23-km visibility), with total column water vapor of 2.9cm and line-of-sight viewing of 45°. The transmission functions corresponding to molecular scattering, aerosol scattering and absorption are also shown in this figure. By examining the atmospheric transmission functions, we can have some general ideas for applications of the MODIS bands. Those bands in transparent atmospheric windows are designed for remote sensing of surface properties. Other bands are mainly for atmospheric studies. The exact location and bandwidth of MODIS bands are selected to meet the requirements from atmospheric, ocean and land sciences. MODIS will provide images of daylight reflection and day/night emission of the Earth, repeating global coverage every 1-2 days. It uses 12 bits for quantization in all bands. The thermal infrared bands have an IFOV (instantaneous field-of-view) of approximately 1 km at nadir. MODIS will view cold space and a full-aperture blackbody before and after viewing the Earth scene in order to achieve calibration accuracy of better than 1% absolute for thermal infrared bands. MODIS is particularly useful because of its global coverage, radiometric resolution and dynamic ranges, and accurate calibration in multiple thermal infrared bands designed for retrievals of SST, LST and atmospheric properties. Specifically, all atmospheric channels of MODIS will be used to retrieve atmospheric temperature and water vapor profiles [Smith et al., 1985], band 26 will detect cirrus clouds, and thermal infrared bands 20, 22, 23, 29, 31-33 will correct for atmospheric effects and retrieve surface emissivity and temperature. Multiple bands in the mid-

infrared range will provide, for the first time, corrections for solar radiation in daytime LST estimations using mid-infrared data. Because of its multiple bands in the mid-infrared range and in the 8-14 μm window, MODIS provides an unprecedented opportunity to develop a physics-based algorithm to simultaneously retrieve surface emissivity and temperature. In Section 2, we present the theoretical basis of the new LST algorithm. Section 3 describes numerical methods used in the algorithm. Section 4 gives simulation results of the new LST algorithm and results from sensitivity and error analysis. In Section 5, we investigate several issues related to the day/night LST algorithm (uncertainties in day/night registration and in surface emissivity changes caused by dew occurrence, and the cloud cover). In Section 6, we present validation results of the LST algorithms with MODIS Airborne Simulator (MAS) dada and ground-based measurement data in two field campaigns conducted in Railroad Valley playa, NV in 1995 and 1996. Finally, the status of MODIS LST software is described in Section 7.

2. *Theoretical Basis of the New LST Algorithm*

For land covers with variable and unknown emissivities, there is greatly insufficient mathematically under-determined information to retrieve surface temperature and band-averaged emissivities from a one-time measurement of N thermal infrared channels. This is so, even when atmospheric temperature and humidity profiles are known exactly, there are still N + 1 unknowns (N band emissivities plus surface temperature). Therefore, we will consider using multi-temporal and multi-channel data.

2.1 A Physics-Based Day/Night LST Model

In clear-sky conditions, the spectral infrared radiance $L(\lambda, \mu)$ at the top of the atmosphere is composed of surface thermal emittance, thermal path radiance $L_a(\lambda, \mu)$, path radiance resulting from scattering of solar radiation $L_s(\lambda, \mu, \mu_0, \phi_0)$, solar beam and downward solar diffuse radiation and atmospheric thermal radiation reflected by the surface,

$$L(\lambda, \mu) = t_1(\lambda, \mu)\, \varepsilon(\lambda, \mu)\, \mathrm{B}(\lambda, T_s) + L_a(\lambda, \mu) + L_s(\lambda, \mu, \mu_0, \phi_0) + t_2(\lambda, \mu, \mu_0)\, \mu_0\, \mathrm{E}_0(\lambda) f_r(\mu; \mu_0, \phi_0)$$

$$+ \int_0^{2\pi} \int_0^1 \mu' f_r(\mu; \mu', \phi') [t_3(\lambda, \mu) L_d(\lambda, -\mu', \phi') + t_4(\lambda, \mu) L_t(\lambda, -\mu', \phi')]\, d\mu'\, d\phi', \qquad (1)$$

where μ is cosine of the viewing zenith angle, $\varepsilon(\lambda, \mu)$ is the surface spectral emissivity, $\mathrm{B}(\lambda, T_s)$ is the radiance emitted by a blackbody at surface temperature T_s, $E_0(\lambda)$ is the spectral solar irradiance incident on the top of the

atmosphere (normal to the beam), μ_0 is cosine of the solar zenith angle, ϕ_0 is the relative azimuth between the viewing direction and the solar beam direction, $f_r(\mu;\mu',\phi')$ is the BRDF function, $L_d(\lambda,-\mu',\phi')$ is the downward solar diffuse radiance, $L_t(\lambda,-\mu',\phi')$ is the atmospheric downward thermal radiance, their incident direction is represented by $-\mu'$ and ϕ', and $t_i(\,)$, $i = 1,\ldots,4$ are transmission functions for the corresponding terms.

The wavelength, λ, in eq. (1) is the wavelength center of a narrow wavelength interval because there is no way to measure the exact monochromatic signal as a continuous function of wavelength by satellite sensors. Equation (1) is the generalized form used in the 8-14 μm thermal infrared range [Wan and Dozier, 1990] into a wider wavelength range of 3-14μm. It requires complete calculations of the atmospheric radiative transfer to determine the values of all terms on the right-hand side. After the zenith and azimuth dependent radiance at user-defined levels from the Earth's surface to the top of the atmosphere (TOA) is provided by accurate atmospheric radiative transfer simulations, the TOA radiance can be represented by its components in form (1). Its special form has been used for a long time in many atmospheric radiation models including LOWTRAN [Kneizys et al., 1983], MODTRAN [Berk et al., 1987], and MOSART models [Cornette et al., 1994]. In the special form, $t_3(\lambda,\mu) = t_1(\lambda,\mu)$ and $t_4(\lambda,\mu) = t_1(\lambda,\mu)$ are assumed.

In order to retrieve surface emissivity and temperature from eq. (1), we need to use suitable TIR bands. According to the MODIS band specifications in Table I and the atmospheric transmission in Fig. 1, bands 20, 22, and 23 are in the transparent atmospheric window in the 3.5-4.2 μm medium wavelength range, bands 29-32 are in the 8-13 μm atmospheric window range, while band 33 is just on the edge of this atmospheric window. Band 30 is strongly affected by ozone absorption, so using this band does not help to retrieve surface temperature. As shown in Fig. 1, major absorbers in bands 20, 22, and 23 are CO_2, N_2, and water vapor. Major absorbers in bands 29, and 31-33 are water vapor and CO_2. The transmission corresponding to aerosol scattering and absorption in these bands is in the range of 0.95-0.98. So using average aerosol distribution in atmospheric radiative transfer is usually good enough unless volcano eruptions strongly change the aerosol distribution. Since CO_2 and O_2 mixing ratios are almost constant, their densities are determined by atmospheric pressure and temperature. Water vapor is the most variable absorber in the Earth's atmosphere. Therefore, if we know atmospheric water vapor and temperature profiles, we can calculate all atmospheric terms in the above equation to a quite high accuracy, which is limited mainly by the accuracy of the coefficients of the water vapor continuum and band absorptions. The MODIS sounding channels can be used to retrieve atmospheric temperature and water vapor profiles [Smith et al., 1985; Menzel and Purdom, 1994]. But retrieving atmospheric profiles needs the knowledge of surface

emissivity in order to separate the surface contribution from the sounding data. Therefore, the retrieved profiles might not be accurate in areas where surface emissivities are highly variable such as in semi-arid and arid areas. Although the absolute values of the retrieved profiles are not accurate, the shapes of the atmospheric temperature and water vapor profiles may be reasonably well obtained. Radiative transfer simulations show that the radiance at the top of the atmosphere, in MODIS TIR bands 20, 22, 23, 29, 31-33, is almost not affected by changing atmospheric temperature and water vapor profiles at levels above 9km elevation because the values of water vapor content at these levels are very low. If the shapes of temperature and water vapor profiles in the lower troposphere can be well retrieved from the MODIS sounding data, we can use two variables to describe the atmospheric variations. One is the amount of shift in the temperature profile up to 9km elevation. Another is the scale factor for the water vapor profile so that we can determine the column water vapor with the shape and the scale factor. Then we use the atmospheric temperature at the surface level, T_a, as the representative variable of the tropospheric temperature profile. Similarly, we can use the column water vapor (cwv) as the representative for the water vapor profile. Alternatively, we can consider it as the first order of approximation to describe the atmospheric condition by using these two variables.

In order to make practical use of multi-temporal and multi-channel data, we need to simplify eq. (1) by using some realistic assumptions about the surface optical properties. We assume: 1) The surface emissivity changes with vegetation coverage and surface moisture content. However, it does not significantly change in several days unless rain and/or snow occurs during the short period of time - particularly for bare soils in arid and semi-arid environments (for which the surface of the ground is normally dry) [Kerr et al., 1992]. 2) There are quite strong spectral variations in surface reflectance for most terrestrial materials in the 3.5-4.2μm wavelength range [Salisbury and D'Aria, 1994], but their BRDF anisotropic factor in this wavelength range has very small variations in the order of 2% [Snyder and Wan, 1996(b); Snyder and Wan, 1996(c)]. So it seems appropriate to assume that a single BRDF anisotropic factor can be used for the surface-reflected solar beam in MODIS bands 20, 22 and 23 located in this wavelength range. This anisotropic factor is defined by the ratio of the surface-reflected solar beam at the view direction of the MODIS sensor to the radiance that would have resulted if the surface reflected isotropically (such a surface is called Lambertian surface),

$$\alpha = \frac{\pi f_r(\mu; \mu_0, \phi_0)}{r} \quad , \tag{2}$$

where r is reflectance of the assumed Lambertian surface. 3) Atmospheric radiative transfer simulations show

that in clear-sky conditions the surface-reflected diffuse solar irradiance term is much smaller than the surface-reflected solar beam term in the thermal infrared range, and the surface-reflected atmospheric downward thermal irradiance term is smaller than surface thermal emission. So the Lambertian approximation of the surface reflection does not introduce significant error in the 3-14 μm thermal infrared region. Then we can replace the BRDF function $f_r(\mu, \mu', \phi')$ in eq. (1) with r/π and link it to the surface emissivity ε by $r = 1 - \varepsilon$ according to Kirchhoff's law.

It is important to point out that in eq. (1) we separate the surface-reflected solar beam term from its irradiance term (the integral of the downward solar diffuse radiance) because changing solar zenith angle has different effects on these two terms. As solar zenith angle increases, the solar beam at the surface level decreases, but the downward solar diffuse irradiance may increase in some situations. If the solar beam is included in the total solar irradiance incident on a surface and surface reflectance (also called as hemispherical reflectance or albedo in the visible and near-infrared range) is defined as the ratio of the total solar radiance reflected from the surface to the total solar irradiance, the surface reflectance will be dominated by the BRDF of the solar beam and therefore the reflectance significantly depends on solar zenith angle [Schaaf and Strahler, 1993]. After the solar beam is separated from the total downward solar irradiance, we can use the BRDF anisotropic factor to calculate the surface-reflected solar beam and use the surface reflectance to calculate the surface-reflected solar downward irradiance. In this way, the solar angle and viewing angle dependences in the surface reflectance will be smaller so that we can assume the surface as a Lambertian surface.

Based on above assumptions, we have developed the following physics-based day/night LST model from eq. (1). The radiance measured in MODIS band j can be expressed as

$$L(j) = t_1(j)\,\varepsilon(j)\,B_j(T_s) + L_a(j) + L_s(j) + \frac{1-\varepsilon(j)}{\pi}\left[t_2(j)\,\alpha\,\mu_0\,E_0(j) + t_3(j)\,E_d(j) + t_4(j)\,E_t(j)\right], \qquad (3)$$

where all terms are band-averaged, $\varepsilon(j)$ is the band emissivity which will be given in eq. (5), similarly for $B_j(T_s)$, $L_a(j)$, $L_s(j)$, and $E_0(j)$. $E_d(j)$ and $E_t(j)$ are the band-averaged solar diffuse irradiance and atmospheric downward thermal irradiance at surface. And $t_i(j)$, $i = 1, .., 4$ are the band effective transmission functions weighted by the band response function, the corresponding radiance, and irradiance terms. Note that we have neglected the in-band spectral variation of the surface emissivity in reducing eq. (1) into eq. (3), and have omitted symbols of view angle and solar angle for most terms in the above equation. On the right-hand side of this equation, $\varepsilon(j)$, α, and $B_j(T_s)$ depend on surface properties and conditions, all other terms depend on atmospheric

water vapor and temperature profiles, solar angle and viewing angle. These terms can be given by numerical simulations of atmospheric radiative transfer. The spectral response functions measured from the Engineering Model of the MODIS instrument have been used as weights in calculations of band averages of these terms.

If we use two measurements (day and night) in N MODIS TIR bands, we have 2N observations. The number of unknown variables are N band emissivities, daytime surface temperature T_{s-day}, nighttime surface temperature $T_{s-night}$, four atmospheric variables (T_a and cwv at two times), and the anisotropic factor α, totalling N + 7. The number of observations must be equal to or larger than the number of unknowns,

$$2N \geq N + 7 \quad . \tag{4}$$

So $N \geq 7$. Note that it is necessary to apply independent shapes of atmospheric temperature and water vapor profiles for daytime and nighttime so that temporal variations and temperature inversion (more often at night) could be considered in the LST retrieval. For the MODIS LST algorithm, these seven bands are MODIS bands 20, 22, 23, 29, 31-33. According to the experience from the Engineering Model of the MODIS instrument, the NEΔT in band 33 may be reduced from 0.25°K to 0.12°K, and it appears possible to achieve the goal for absolute calibration accuracy, 0.5-0.75%, for these seven TIR bands. It seems that we can get unique solutions for the above 14 unknowns using 14 observations. But it is actually not true because: 1) the atmospheric profile is a continuous function of height and there are only a finite number of MODIS sounding bands so that the atmospheric temperature and water vapor profiles can be retrieved only at a finite number of levels, 2) there are always uncertainties in the retrieved atmospheric profiles and even in their shapes, 3) there is always instrument noise in the measurement data, 4) there are uncertainties in the atmospheric optical properties including water vapor absorption coefficients which we used in the development of LST algorithms. Therefore all we can do is to use a best combination of available bands and use an appropriate method to determine the best estimates of the unknown variables. We also need to use enough a priori knowledge and constraints of the atmosphere and the surface as "virtual measurements" to make the retrieval problem well posed [Rodgers, 1976]. The advantage of using daytime data in MODIS bands 20 and 22-23 is that solar radiation can be used as TIR source in the medium wavelength range so that the day/night LST model is essentially an active method to get the information of surface reflectance. Combining with the nighttime data in these three bands and day/night data in the other four MODIS bands makes it possible to simultaneously retrieve surface emissivity and temperature. The advantage of including four atmospheric variables (T_a and cwv in daytime and nighttime) is that atmospheric variations are considered in the retrieval procedure so that uncertainties in the initial atmospheric conditions could be reduced

and a better self-consistent solution of the surface emissivity and temperature could be reached.

2.2 Band-Averaged Emissivities of Land-Surface Materials

The band-averaged emissivity is defined as

$$\varepsilon(j) = \frac{\int_{\lambda_{j,L}}^{\lambda_{j,U}} \Psi(\lambda)\,\varepsilon(\lambda)\,d\lambda}{\int_{\lambda_{j,L}}^{\lambda_{j,U}} \Psi(\lambda)\,d\lambda} \tag{5}$$

where $\Psi(\lambda)$ is the spectral response function of band j, $\lambda_{j,L}$ and $\lambda_{j,U}$ are its lower and upper boundaries. By using MODIS spectral response functions, band-averaged emissivities can be calculated from published spectral reflectance data of 80 pure terrestrial materials [Salisbury and D'Aria, 1992 and 1994]. This spectral data base includes igneous, metamorphic, and sedimentary rocks, varnished rock surfaces, lichen-covered sandstone, soil samples, green foliage, senescent foliage, water, ice, and water surfaces with suspended quartz sediment or oil slicks. The sample names and numbers are listed in Table II. The calculated band emissivities in MODIS bands 20, 22, 23, 29, 31-33 are shown in Fig. 2. The sample number corresponds to the sample name and the type of material in Table II. As shown in this figure, there are very strong variations in the band emissivities for rock and sand samples, and for some soil samples and senescent vegetation foliages. For example, the emissivity of sands in MODIS band 20 could be as low as 0.55. However, the band emissivities in MODIS bands 31-33 are larger than 0.8 for all samples in the spectral reflectance database. For water, ice, and green vegetation leaves, there are small emissivity contrasts among these seven bands and their band emissivities vary in small ranges.

2.3 Atmospheric Radiative Transfer Simulations

The accuracy of atmospheric radiative transfer numerical models depends on numerical methods to solve the radiative transfer equation and both our knowledge of the atmosphere and its inherent optical properties [Goody and Yung, 1989]. The many methods available to solve the atmospheric radiative transfer problem have proved their fundamental theory and mathematically interesting because there are important applications in neutron diffusion theory, astrophysics, and earth sciences. For example, there are a variety of methods based on two-stream approximations [Meador and Weaver, 1980; Tanré et al., 1990], 4-stream approximations [Cuzzi et al., 1982], and others such as delta-M method [Wiscombe, 1977], adding/doubling method [Wiscombe, 1976], discrete ordinate method [Stamnes and Conklin, 1984], and Monte Carlo simulation method [Adams and

Kattawar, 1978]. We developed a radiative transfer model, which provides accurate matrix solutions of the azimuth-dependent scalar radiative transfer equation for a vertical inhomogeneous, multi-layer atmosphere by using the adding/doubling method for the development of algorithms to estimate column ozone and LST in clear-sky conditions [Smith et al., 1992; Wan and Dozier, 1989; Wan and Dozier, 1996]. Results from this model match those from Stamnes and Conklin's discrete-ordinates [Stamnes and Conklin, 1984] calculations to four decimal places. Atmospheric radiative models based on the adding/doubling method have advantages in easy implementation of surface interfaces, such as the air-water interface and interfaces for specular reflectance or BRDF reflectance, and in efficiently getting solutions for multiple boundary conditions.

The continuous update of the LOWTRAN code [Kneizys et al., 1983; Kneizys et al., 1988] and MODTRAN code [Berk et al., 1987; Berk et al., 1989] developed by the U.S. Air Force Geophysics Laboratory over the past two decades represents a significant progress in improving our knowledge of optical properties of the earth's atmosphere. A two-stream approximation with multiple scattering parameterization [Kneizys et al., 1988; Isaacs et al., 1987] is used in the LOWTRAN model. The new versions of MODTRAN code have the option to use the discrete ordinate method.

In the TIR range, LOWTRAN7 [Kneizys et al., 1988] and MODTRAN [Berk et al., 1989] give transmission functions of each molecule at a wavenumber interval of $5cm^{-1}$ and $1cm^{-1}$, respectively. The LOWTRAN7 band model was based on a least squares fitting to FASCODE [Clough et al., 1986] calculations of various transmittances, but MODTRAN is based on a separate band model, derived directly from the HITRAN [Rothman et al., 1992] data base, by-passing FASCODE. The MODTRAN band model has been validated against spectrally degraded FASCODE calculations for both radiance and transmittance. The agreement is usually within a few percent RMS and seldom exceeds 5% [Wang et al., 1996]. Note that non-monochromatic transmission values cause a violation of the Lambert-Bouguer-Beer law because of the complexity of molecular band absorption. This is true even for a narrow wavenumber interval of 1 cm^{-1}. One solution to this problem is to expand radiative transmission functions calculated from LOWTRAN or MODTRAN by using "exponential-sum fitting" [Wiscombe and Evans, 1977]. Following this technique the monochromatic radiative transfer model [Chandrasekhar, 1960] is applied separately to each term in the exponential-sum expansion, and the results summed. After convoluting these results with the spectral response function, we can get band-averaged atmospheric terms in eq. (3). A radiative transfer code using the "exponential-sum fitting" formulation has been implemented successfully on workstations and massive parallel computers, and the simulation results have been

used in the development of a generalized split-window LST algorithm [Wan and Dozier, 1996]. Typically, the total number of the cross-product terms in the exponential-sum fitting formulation is over 1,000 so it is very computationally time consuming. The advantage in using the exponential-sum fitting formulation is that we obtain more accurate results. For example, the resulted three effective transmission functions for the viewing path in eq. (1) may be different by a few percent ($t_3 > t_1$ and $t_4 < t_1$) because of selective, wavelength-dependent molecular band absorption. This occurs even though these transmission functions are defined for a same optical path from the target to the top of the atmosphere in the viewing direction of the sensor. The correlated-k distribution method [Lacis and Oinas, 1991; Fu and Liou, 1992] is an alternative to the exponential-sum-fitting method. Usually the number of terms used in the correlated k-distribution method is smaller so that it is computationally efficient and it gives accurate results. The multiple scattering algorithm in the MODTRAN code is being upgraded to include a "correlated-k" absorption characterization.

As shown in Fig. 1, the atmospheric transmission in the 8-13 μm window, where three MODIS bands are located for the purpose of remote measurements of surface temperature, strongly depends on water vapor absorption including band absorption and continuum absorption. A review for measurements of water vapor absorption in the 8-13 μm atmospheric window reveals a considerable variation in its magnitude over the past 20 years [Grant, 1990]. The accuracy of water vapor continuum absorption in five of the measurements reviewed is approximately 10%, adequate experimental measurements are lacking at temperatures below 280 °K. There is no accepted theory for the continuum absorption. Recent theoretical studies [Ma and Tipping, 1992; Ma and Tipping, 1994] on water vapor continuum absorption have led to significant progress in understanding the physical mechanisms and the temperature dependence of the continuum absorption. But it is still premature to theoretically determine the magnitude and the temperature dependence of the water vapor continuum absorption coefficients. Thus, modelers must rely on empirical formulations [Robert et al., 1976; Clough et al., 1989] based on laboratory measurements [Burch and Alt, 1984]. Atmospheric conditions, especially cold temperatures and/or high humidities, are difficult if not impossible to reproduce in the laboratory. This is particularly true in the vital area of continuum absorption. Studies at relative humidities over 70% are a persistent problem. This is the threshold for condensation on hygroscopic dust particles and therefore for fogging of optical elements. Furthermore, laboratory spectroscopists have almost reached an impasse in the area of line wings and the continuum that prevents progress in line-by-line modeling [Varanasi, 1988]. In the past several years, the water vapor absorption has been compared and validated with High-Resolution Interferometer Sounder (HIS) spectral radiance data involving vertical path measurements from an aircraft, as well as from the ground [Clough et al.,

1989; Smith et al., 1993], and long-path atmospheric transmission measurements [Thériault et al., 1994]. The empirical continuum formulation used in the FASCODE code [Clough et al., 1986], as well as in LOWTRAN and MODTRAN codes has been changed several times in the past decade. In the LOWTRAN7 code [Kneizys et al., 1988] and earlier versions of the MODTRAN code [Berk et al., 1987], the magnitude of the water vapor self continuum absorption coefficient in the 8.5-13 μm window is smaller by approximately 20% compared to that used in the LOWTRAN6 code [Kneizys et al., 1983]. Clough [1995] made a new correction to the the water vapor continuum based on the measurement of the downwelling radiance at Kavieng, New Guinea by Westwater et al. [1994], and the measurements by Revercomb and colleagues at the University of Wisconsin. This new continuum formulation has been implemented in version 3 of the MODTRAN code in 1994. Because the uncertainty in the water vapor continuum absorption coefficients may be larger than a few percent, it is not critical to neglect the small differences among transmission functions t_1, t_3 and t_4 in eq. (1) before the accuracy of the water vapor continuum absorption coefficients is significantly improved. So we accept the approximations $t_3 = t_1$ and $t_4 = t_1$ in eq. (1) that are made in the MODTRAN3 code up to its version 1.3 in the time being. The effect of these approximations should be considered along with uncertainties due to other sources when actual data are used to retrieve surface emissivity and temperature. Note that even we assumed that in each narrow spectral interval of 1 cm^{-1} or 5 cm^{-1} the transmission functions for the viewing path are equal in eq. (1), the band effective transmission functions $t_3(j)$ and $t_4(j)$ may still be different from $t_1(j)$ in eq. (3). Keeping in mind all the problems raised above for radiative transfer models, in this study we use version 1.3 of the MODTRAN3 code [Berk et al., 1989] to calculate all atmospheric and solar terms in eq. (3). The discrete ordinate option with eight streams is used in MODTRAN3 calculations so that the effect of multiple scattering due to background aerosols is considered in the calculations of the path radiances and the downwelling irradiances.

The path radiance resulting from scattering of the solar radiation in eq. (3), $L_s(j)$, does depend on the relative azimuth between viewing direction and the solar beam direction. This dependence is determined by the aerosol loading, its size distribution, type and scattering phase function. The aerosol information and properties are not readily available in most situations. As shown in Fig. 1, the total aerosol effect on the transmission function in the thermal infrared range is small in normal clear-sky conditions. Radiative transfer simulations indicate that the value of L_s is only several hundredths of the direct solar beam value at the surface level, and that the azimuth dependence in L_s is less than 10%. So it is appropriate to neglect this azimuth dependence and to use the azimuth-averaged value of L_s in the new LST algorithm.

2.4 Variations of Atmospheric Conditions

It is important that a practical LST algorithm should accommodate atmospheric variations in a range that is wide enough to cover all possible real situations. For LST retrieval, we only consider atmospheric variations in clear-sky conditions. In the thermal infrared range, the most important atmospheric variables are atmospheric water vapor and atmospheric temperature profiles. Atmospheric absorption and thermal emission occur mainly in the lower troposphere. We assume that the MODIS product of the atmospheric temperature and water vapor profiles retrieved from MODIS sounding channel represents the shapes of the profiles well but maybe does not represent their absolute values because of the difficulties in decoupling the atmosphere-land interaction. Atmospheric temperature and water vapor at any level will be interpolated from their values retrieved at fixed levels. Given the shapes of temperature and water vapor profiles, we can use only two variables to describe variations of the clear-sky atmospheric condition: a shift of the temperature profile below elevation 9km, and a scaling factor for the water vapor profile. The column water vapor can be determined by the shape and the scaling factor. In order to build a data base for the atmospheric and solar terms in eq. (3), we will select 24 basic atmospheric profiles considering different shapes of temperature and water vapor profiles, and the range of air surface temperatures in different regions and seasons. Some basic atmospheric profiles include temperature inversion layers. Then we add more variations to each of these basic atmospheric profiles in the following ways: 1) A δT is added to the atmospheric temperature profile at all levels between surface and elevation 9km, δT varies from -10 °K to +20 °K in steps of 2 °K. The modified atmospheric temperature at the surface level, T_a, will be used as representative of the entire atmospheric temperature profile. 2) The atmospheric water vapor profile at all levels between surface and elevation 9km is scaled in steps of 10% so that the column water vapor varies from 10% to 120% of the basic value.

2.5 Variations of the Land-Surface Temperature

In the simulation study of the new LST algorithm, we consider LST variations in a wide range of LST variations. The daytime surface temperature varies from atmospheric surface temperature T_{a-day} to T_{a-day} + 24 °K in steps of 6 °K, and the nighttime surface temperature varies from $T_{a-night}$ – 13.5 °K to $T_{a-night}$ + 4.5 °K in steps of 4.5 °K.

3. *Numerical Methods Used In The New LST Algorithm*

3.1 Look-Up Table Method

In order to save computational time on numerical simulations of atmospheric radiative transfer for calculating the atmospheric and solar terms in eq. (3), look-up tables will be used in the new LST algorithm. In this way, we only need to make a complete series of radiative transfer simulations once to build these look-up tables. Because multi-dimension interpolations are involved in our look-up table method, linear interpolation is most efficient. This requires smaller intervals (or steps) for these look-up tables. For example, the step for the atmospheric temperature variation is 2 °K, the step for atmospheric column water vapor is 10% of the average value, the step for solar zenith angle and viewing zenith angle is 10 ° for angles smaller than 30 ° and 5 ° for larger angles. The upper limits for solar and viewing zenith angles are 75° and 65°, respectively. Similarly, a look-up table in a step of 0.1 °K is also built for the band-averaged Planck functions in the temperature range 200-400 °K, which is the maximum dynamic range for the seven MODIS bands used in this LST algorithm. It is required that errors caused by look-up tables and interpolation methods should be smaller than NEΔT. If this resolution scheme is used to build a look-up table for the three solar terms in eq. (3) for 24 basic atmospheric profiles, the total size of the look-up table is approximately 60MB. If use of small look-up tables is a higher priority, we can use 3-point interpolation method so that six zenith angles are enough for viewing and solar angles. However, 3-point interpolation takes much more computational time than linear interpolation. The sizes of look-up tables for the other three atmospheric terms (transmission, thermal infrared path radiance, and downward thermal infrared irradiance) are much smaller.

3.2 Approaches to Solve the Retrieval Problem

We have developed two approaches to solve the LST retrieval problem. The first one uses statistical regression method, and the second one uses other numerical methods to solve the set of nonlinear eq. (3).

In a linear approximation of eq. (3) in the proximities of reference values of surface temperature and band emissivities, the left-hand side reduces to the band brightness temperature and the right-hand side reduces to surface temperature and band emissivities. Combining 14 equations together, the solution for surface temperature and band emissivities should be a linear combination of the band brightness temperatures, each of which corresponds to one of the 14 observations. Its mathematical form is

$$x_i = \sum_{j=1}^{14} w_{i,j}\ y_j + w_{i,0}\ , \tag{6}$$

where x is a vector of the 14 variables including surface temperatures and band emissivities, y_j is the band brightness temperature for observation j, and $w_{i,j}$, i = 1, ..., 14 and j = 1, ..., 14 are coefficients. And $w_{i,0}$ is the coefficient for the offset term. We can determine these coefficients in two steps. In step 1, we construct a large set of simulated observation values in wide ranges of atmospheric and surface conditions. In step 2, we make a statistical regression analysis using the band brightness temperatures associated with these simulated band radiance values as independent variables and using the given surface band emissivities and temperatures, and atmospheric parameters as dependent variables. The output of this regression analysis will be the coefficients in eq. (6). The process of statistical regression analysis takes much computational time. But it needs only to be done once. The values of x_i provided by this approach are the best estimates of these unknown variables in the statistical sense.

If we have better information on the shapes of the atmospheric temperature and water vapor profiles for the time which makes it possible to have a clear-sky day/night pairs of MODIS data, we can use other methods to numerically solve the set of nonlinear eq. (3). We tried the Quasi-Newton method [Dennis and Schnabel, 1993] and the Least-Squares Fit (χ^2 fit) method [Bevington 1969]. As Rodgers [1976] pointed out, retrieval problems in remote sensing are generally nonlinear. The main sources of the nonlinearity in eq. (3) are: 1) temperature dependence of the atmospheric transmission, 2) the dependence of transmission on absorber concentration, 3) temperature dependence of the Planck function, 4) wavelength dependence of the Planck function across a spectral band, 5) wavelength dependence of the Planck function between spectral bands, and 6) nonlinear constraints.

The initial values of the 14 unknown variables are given in their constrained ranges based on reasonable guesses or statistical analysis. The Quasi-Newton method is slightly more computationally efficient. These two methods give similar results in cases not including noise. It is well known [Bevington, 1969; Dennis and Schnabel, 1983] that global convergence to right solutions is not guaranteed for nonlinear problems, especially when noise is included. The χ^2 fit method is selected in the new LST algorithm because it is more stable in our simulation studies. We are only interested in real situations where there is noise in remote measured data caused by the intrinsic instrument sources and actual turbulence and fine structure in the atmosphere.

A measure of the goodness of χ^2 fit is defined by [Bevington, 1969]

$$\chi^2 = \sum_{j=1}^{14} \{ \frac{1}{\sigma_j^2} [L_j - L(j)]^2 \} , \tag{7}$$

where L_j is the scaled band radiance observation value, j = 1, 7 for daytime, j = 8, 14 for nighttime. $L(j)$ is the scaled band radiance function in eq. (3), which depends on unknowns x_i , i = 1 , 14. We use the values of band-averaged Planck functions at a reference temperature, 300 °K, to scale the band radiance in corresponding bands so that the scaled differential radiance may be comparable. The term σ_j is the uncertainty in observation value L_j. In cases without noise, σ_j is identically equal to 1. However, for cases which include noise NEΔT, σ_j will be

$$\sigma_j = L_j \frac{n_j \, \Delta T_{neq}(j)}{T_b(j)} \tag{8}$$

based on the following approximation for the band-averaged Planck function

$$L_j \simeq C_j \, T_b^{\,n_j}(j) \tag{9}$$

where $\Delta T_{neq}(j)$ is the NEΔT value in band j, and $T_b(j)$ is the brightness temperature corresponding to band radiance L_j. In the temperature range 240-400 °K, regression analysis gives the best fitting values for n_j, they are 12.91, 12.25, 11.98, 6.00, 4.70, 4.11, and 3.74 for MODIS bands 20, 22, 23, 29, 31-33. Note that this approximation is used only in calculation of σ_j, which determines the weight in eq. (7). The effect of errors caused by this approximation on solutions is negligible.

One of the difficulties in the χ^2 fit processing is that there may be more than one local minimum for χ^2 within a reasonable range of values for variable x_i, particularly in cases including noise. Therefore the final solution may depend on their initial values. We use two different ways to make the initialization. In the first way, we use a dozen sets of initial values that are spread over preassigned ranges all from minimums to maximums to get different solutions and select the solution associated with the minimum χ^2 value. In noisy situations, this selected solution may not be the best one we searched for. An alternative way is to use the estimates provided by the statistical regression method as the initial values. We use the second way in our LST algorithm. Typically, the χ^2 fit method takes 3-4 iterations to reach the final solution.

4. *Sensitivity and Error Analysis*

Using look-up tables, we can quickly construct 14 band radiance values (seven values for daytime and seven values for nighttime) at the top of the atmosphere for any given conditions of surface band emissivities and BRDF anisotropic factor, daytime and nighttime surface temperatures, daytime and nighttime atmospheric surface temperatures and column water vapor values, solar angle and viewing angle. Then we can use these 14 radiance values as simulated MODIS observations to retrieve the given surface and atmospheric variables. We can then construct a sensitivity and error analysis, presented in the following sub-sections.

4.1 Errors Due to Look-up Table and Interpolation Methods

In the first numerical simulation experiment, we do not include any noise in the data construction in order to test the numerical method to solve the nonlinear problem and to evaluate the errors caused by the use of look-up tables and interpolation methods. We use the temperature and water vapor shapes in the "average" mid-latitude summer atmospheric profiles (model 2 in MODTRAN) and set the daytime and nighttime atmospheric surface temperatures at 298.2 °K and 290.2 °K. The column water vapor is set at 2.6cm for both daytime and nighttime for simplicity. In real applications, we use independent variables for the column water vapor in daytime and nighttime. We set the anisotropic factor as 1, solar zenith angle at 45 °, viewing angle at nadir for daytime and nighttime, five different daytime surface temperatures ranging from 298.2 °K to 322.2 °K, and five different nighttime surface temperatures ranging from 276.7 °K to 294.7 °K. There are 25 cases of different daytime and nighttime surface temperatures for each sample of 80 surface materials. The band emissivities of these 80 terrestrial material samples cover the range from 0.55 to almost unity. The standard deviations of errors in retrieved surface temperatures are 0.27 and 0.21 °K for daytime and nighttime, the standard deviations of errors in retrieved emissivities are in 0.005-0.008 for bands 1 to 6, and 0.012 for the last band because of the low transmission of MODIS band 33 in the atmospheric condition. The standard deviations of errors in retrieved BRDF anisotropic factor, atmospheric temperatures, and column water vapor are 0.08, 0.10-0.15 °K, and 0.06cm, respectively. These numbers indicate that look-up tables are appropriate and the χ^2 fit method works well.

4.2 Sensitivities to the Uncertainties in Atmospheric Profile Shapes

In the second simulation experiment, we set the NEΔT values for the seven bands at 0.05, 0.07, 0.07, 0.05, 0.05, 0.05, and 0.12 °K, set 0.5% as the systematic calibration error for all bands, and keep all other parameters as in the first experiment. In our simulation, NEΔT is treated as a random noise. We consider four different

atmospheric conditions in mid-latitude summer, one is the "average" condition used in MODTRAN code (model 2), two (labeled by A109 and A117) are selected from the satellite TOVS Initial Guess Retrieval (TIGR) atmospheric profile database [Moine et al., 1987], and the fourth (labeled by "average-4K") is the variant of the "average" one by shifting -4 °K on the temperature profile but keeping its water vapor profile unchanged. As shown in Fig. 3, three of them have almost the same air temperature at the surface level, but they have very different shapes in the temperature and water vapor profiles. The temperature discrepancy between the "average" profile and profile A109 may be as large as 10 °K at elevations near 2km and between 6-10km. The difference in water vapor profiles in atmospheric conditions of "average", A109, and A115 may be 20% to 50% or even larger. We established separate data bases of the atmospheric terms in eq. (3) through atmospheric radiative transfer simulations for these different atmospheric conditions. The separate data bases will be used to calculate the daytime and nighttime band radiances in the seven MODIS bands in wide ranges of surface temperature for 80 surface samples. These calculated band radiances are then used as simulated observations. The coefficients in eq. (6) were obtained by statistical regression analysis of the observations simulated for the "average" atmospheric condition. We suppose that there is enough information available for the "average" atmospheric condition, but there is no information available on the shapes of the atmospheric profile for atmospheric conditions likes those in A109 and A115. In the statistical approach, we apply the same set of regression coefficients to the four sets of simulated observations data for retrieving surface temperatures and emissivities. In the χ^2 fit approach, these surface temperatures and band emissivities retrieved by the regression approach are used as initial values for further iterative processing. The standard deviations of errors in surface temperatures and band emissivities retrieved by the statistical regression method are given in the first part of Table III, and those retrieved by using the χ^2 fit method are given in the second part. Comparing the results from the statistical approach and χ^2 fit approach for the "average" atmospheric condition indicated that the χ^2 fit method gives significant improvements on retrieved surface temperatures and band emissivities. This is because we know the shapes of the atmospheric temperature and water vapor profiles well enough to select the right set of the regression coefficient and the right parts from the look-up tables for the atmospheric and solar terms in eq. (3). But for atmospheric conditions A109 and A115, we do not have the information for making the right selections. So the results retrieved from the χ^2 fit approach are worse than those from the statistical approach. However, for the case with the shifted "average" temperature profile, the standard deviations of errors in surface temperatures retrieved by using the χ^2 approach is reduced by a factor of 2, and the accuracies of retrieved band emissivities are improved by almost 50% because the shapes of atmospheric temperature and water vapor profiles in this case

are as same as those in the "average" profile. From this experiment we gained the following insights: the statistical method is less accurate but is also less sensitive to uncertainties in the atmospheric profile shapes; and the χ^2 fit method may be more accurate but is more sensitive to uncertainties in the profile shapes. In the following part of this paper, we assume that the information of the profile shapes is available so that it is appropriate to pursue the χ^2 fit approach.

4.3 Sensitivities to the Three Assumptions of Surface Optical Properties

In the first test, C1, of the third simulation experiment, we set the NEΔT values for the 7 bands at 0.05, 0.07, 0.07, 0.05, 0.05, 0.05, and 0.12 °K, set 0.5% as the systematic calibration error for all bands, and kept all other parameters as in the first experiment. The errors in surface temperatures retrieved by the χ^2 fit method for a total of 2,000 different cases are shown in Fig. 4A. The errors in retrieved band emissivities in MODIS bands 31 and 32 are shown in Fig. 4B. The standard deviations of errors in retrieved surface daytime and nighttime temperatures are in range of 0.4-0.5 °K, and the standard deviations of errors in band-averaged emissivities in MODIS bands 31 and 32 are 0.009 over a wide range of surface temperatures in the mid-latitude summer atmospheric condition. We can see the effect of the 0.5% systematic calibration error in Fig. 4A. This forces the retrieved temperature to shift to the positive direction by approximately 0.2 °K. The histograms of errors in retrieved surface temperatures and emissivities in bands 31 and 32 for a total of 2,000 cases are shown in Fig. 5A and 5B. We also applied the day/night LST method to "mixed samples" that contain a mixture of two samples of the 80 terrestrial materials at different surface temperatures. Similar results have been obtained as long as band emissivities of the mixed sample are calculated from the components with their proportions as weights and its effective surface temperature is calculated from the total thermal radiation in MODIS band 31. The effective surface temperature of a mixed sample does depend on band number, but this dependence is very small (about the instrument noise level) in normal surface conditions. We do not consider forest fires in the LST processing because the MODIS TIR bands may be easily saturated by subpixel fires at a small size and there is no sufficient knowledge on the optical properties of fires and smoke for making atmospheric corrections. In test C1 of this experiment, the maximum error in the retrieved LST is 3.2 °K for only one case (for the Indian grass sample at temperature 322.2 °K). Without considering this extreme case, the maximum error in retrieved LST will be 2.2 °K. Note that we simulated the surface temperature variation in a very wide range. For each sample, the surface temperature varies in a range of 24 °K in daytime, and in a range of 18 °K in nighttime. These ranges are too wide for some land covers in real situations. For example, the temperature of snow cover and ice could not be

above a few degrees C. This is so, even considering the possibility of some small proportion of other land covers mixed in the scene, because the temperature of water surface and healthy vegetation is not likely to be warmer than the air surface temperature by 24 °K. Higher solar elevation and surface temperature in a normal range are favorable conditions for land covers with low reflectances. In such situation, the solar beam can be effectively used as an active TIR source for remote measurements of the surface reflectance in the medium wavelength range so that the band emissivities in MODIS bands 31 and 32 can be also retrieved at an accuracy better than 0.01. Then these retrieved emissivities can be used in the generalized split-window LST algorithm [Wan and Dozier, 1996] to quickly retrieve LST of same area for a period of one or more weeks depending on season and weather conditions.

Now we check whether it is possible to relax the three assumptions of surface optical properties made in section 2.1. The first row in Table IV gives standard deviations of the surface temperature and emissivities retrieved in test C1 of this experiment. In tests C2 and C3, we introduce some variations for the nighttime surface band emissivities to simulate its possible change with surface moisture content. In test C2, the nighttime band emissivities increase by 0.01 and they are only limited by its maximum value 1. In test C3, the emissivity increment depends on its value, a lower band emissivity could increase more. This may be the case for sands, its emissivity in MODIS band 20 is 0.56, it could increase to 0.604 at night. The standard deviations of errors in daytime and nighttime surface temperatures, and band emissivities retrieved by the χ^2 fit method are increased slightly. Note that the retrieved emissivities are compared to daytime emissivities only. In tests C4 and C5, we set different BRDF anisotropic factors for the three bands in the mid-infrared range by differences of 5% and 10%. There is no significant change in the retrieved surface temperature and emissivities. In tests C6 and C7, we use non-Lambertian reflectance for the surface-reflected solar diffuse irradiance and atmospheric downward irradiance terms. They differ from the reflectance of a Lambertian surface by ±20%. The effect of the non-Lambertian reflectance is also not significant. Comparing the standard deviations in tests C2 through C7 to those in test C1 shows that the maximum difference in standard deviations of errors in retrieved surface temperatures is 0.17 °K and the maximum difference in standard deviations of errors in retrieved band emissivities is 0.005, they are comparable to or smaller than the effects caused by NEΔT and calibration errors of the instrument. Therefore, we do not need to understand the three assumptions of surface optical properties described in section 2.1 as strict constraints to the new LST algorithm.

4.4 Sensitivities to NEΔT and Calibration Errors

In the fourth simulation experiment, we keep the same atmospheric and surface temperature parameters as the first experiment, but change NEΔT and calibration error values in a series of tests, as shown in Table V. The first column in the table indicates the test number. Seven NEΔT values for seven bands used in the new LST algorithm are listed in the second column block, and a systematic calibration error for all bands in the third column. Standard deviations (δT_s) and maximum errors (ΔT_s) of the retrieved daytime and nighttime surface temperatures are given in columns 4-7. The standard deviations of errors in retrieved emissivities for MODIS bands 31 and 32 are given in the last two columns. Comparison between test D1 and test D2 indicates that the effect caused by a systematic calibration error of 0.5% is comparable to the effect of the given NEΔT values. Test D3 indicates that doubling the NEΔT values increases the standard deviation of retrieved daytime surface temperature by approximately 0.2 °K. Comparing tests D4 and D5 to test D2 indicates that errors in retrieved surface temperatures and band emissivities become larger as the calibration error increases. In order to achieve the 1 °K requirement for the LST accuracy and to retrieve band emissivities in MODIS bands 31 and 32 at an accuracy of the 0.01 level, the calibration error should be smaller than 1%. The new LST algorithm requires small NEΔT (large signal-to-noise ratio) and a high consistent calibration accuracy for the seven bands used. The split-window SST and LST algorithms also need these requirements for MODIS bands 31 and 32. However, the new LST algorithm needs these requirements over a much wider spectral range.

5. Several Issues Related to Day/night Algorithm

5.1 Day/night Registration

It is natural to link the MODIS day/night LST algorithm to the apparent thermal inertia (ATI) algorithm of the Heat Capacity Mapping Mission (HCMM) sensor [NASA, 1980; Short and Stuart, 1982; Price, 1985; Vukovich, 1984; Majumdar and Bhattacharya, 1990]. The HCMM program was the first NASA research effort directed mainly toward observations on the thermal state of Earth's land surface from an unmanned satellite. The HCMM spacecraft operated between April 1978 and September 1980. MODIS is a much more advanced instrument than HCMM in terms of the thermal remote sensing capability except for the spatial resolution, as shown in Table VI. The nature of the analog telemetry system onboard the satellite results in some variability in the quality of the HCMM data and the data quality was also influenced by the quality of the receiving station recording [NASA, 1980]. Because there was only one TIR channel on HCMM, it was not possible to make atmospheric and

emissivity corrections unless in-situ measurements of atmospheric profiles and surface emissivity were available. The ATI algorithm requires data in the 12-hour day and night coverage for estimate the day/night temperature difference. So cloud cover was a hindrance to the accomplishment of objectives [Short and Stuart, 1982]. The MODIS day/night LST algorithm does not require the 12-hour day and night coverage, it can use daytime and nighttime data collected in several days as long as the surface emissivity does not change significantly. Therefore, the chance to have a pair of daytime and nighttime data both in clear-sky conditions will be much large. It does not assume the same atmospheric conditions for daytime and nighttime because separate atmospheric variables are used for day and night.

The uncertainty in day/night registration of MODIS data may be a major error source for the day/night LST algorithm. Numerical simulations have been made to evaluate the sensitivity of the day/night LST algorithm to the uncertainty in day/night registration. We assume that a vegetation component is mixed with another terrestrial material in the 80-sample database. It is assumed that the daytime proportion of the vegetation component in a mixed pixel is 0.5 and the nighttime proportion varies from 0.5 to 0.2 for simulating the mis-registration effect. The daytime canopy temperature of the vegetation component is given three values: the same surface temperature as for the another component, 4 °K warmer or cooler than the surface temperature of the another component. Its nighttime temperature is assumed to be equal to the surface temperature of the another component. The mid-latitude summer atmosphere is used in this simulation study. Note that the same NEΔT values and the systematic calibration error 0.5% used in typical numerical experiments for the day/night LST algorithm are also used in this sensitivity study. The rms and maximum errors in surface temperatures and band emissivities retrieved by the χ^2 fitting day/night LST algorithm are shown in Table VII. The band emissivities of the mixed pixel are calculated from the band emissivities in the database and the proportions. The average values of calculated daytime and nighttime band emissivities are used as the target values for retrieval. Results in Table VII indicate that the day/night LST algorithm still works well as long as the nighttime proportion of the vegetation component is not smaller than 0.35, differing from the daytime proportion by less than 30%. This corresponds to a mis-registration 15% or 30%, depending on how the vegetation component distributed in the mixed pixel.

5.2 The effect of surface emissivity changes caused by dew

Dew is a common global phenomenon. By model calculations and measurements of dew occurrence, Janssen and Römer [1991] showed that there were 220 dewy nights and 1600 dewy hours in the Netherlands in 1987. Six

years of dew observations in the Negev Desert, Israel [Zangvil, 1996] show that the total monthly dew hours is 145 h per month from August to January, and 80 h per month from February to June and that the average duration of dew per dew night appears to follow closely the length of the night. Scherm and Bruggen [1993] used a previously verified and validated model to calculate the frequency and duration of dew occurrence with hourly weather data over a growing season (April-October) in different climate regions of California. Simulation results indicated that high dew occurrence (78-93% of the days) and long mean dew duration (8.7-9.3 per day) at coastal stations, and low occurrence (23% of the days) and short duration (0.9 h per day or 3.7 h per dew event) at the interior valley site. The dew duration is sensitive to changes in humidity and cloud cover at the coastal sites and to humidity and wind speed at the interior valley site. An empirical model to estimate the duration of dew periods by the use of dew point depression, wind speed, and relative humidity (RH) as inputs [Gleason et al., 1994], has an accuracy better by only 5-10% than a simple RH > 90% model [Sutton et al., 1984]. This indicates that the near-surface relative humidity is the primary factor in dew occurrence. Because the weather data are usually not available in remote areas, it is not easy to calculate dew occurrence with the dew models. The near-surface humidity in the MODIS atmospheric profile product may be used to reject the dew occurrence. Considering potential large errors in the temperature and water vapor in the surface boundary layer in the MODIS atmospheric profiles product, RH < 50% may be used as a conservative condition for nondew hours. Then we only need to detect night dew in our LST algorithm in relatively wet conditions (RH > 50%). When dew occurs at night the surface emissivity may be changed significantly if a land cover has a low emissivity in dry conditions, for example, in the desert environment. This significant change in surface emissivity should be shown in TIR data. If surface emissivity at night differs significantly from the value in daytime, the major link between day and night observations used in the day/night LST method will be lost. So we need to find some additional information to help the LST retrieval with only the multiband night-only observation. The empirical relationship between the minimum emissivity (ε_{min}) and the spectral contrast which is described by the maximum-minimum difference (MMD) is such an information. This relationship is used in the ASTER TES algorithm [ATBD-AST-03, 1996]. Based on 80 laboratory reflectance spectra of rocks, soils, vegetation leaves, snow, ice and water [Salisbury and D'Aria, 1992] and their mixed values with three different portions of vegetation (totally 320 samples), two empirical relationships between minimum emissivity (ε_{min}) and the spectral contrast described by MMD (maximum and minimum difference) have been calculated. One is for five MODIS bands (bands 20, 22, 23, 29 and 31), and another for the seven MODIS bands used in the day/night LST algorithm, as shown in Fig. 6. These two relationships have been added to our day/night algorithm as an option.

We also made a series of numerical simulations with the enhanced day/night LST algorithm (called MMD-MIN χ^2 fitting LST method hereafter) in cases with and without night dew. Seven tests have been made to show the performance of three options of this enhanced LST algorithm: night-only, day-only, and day/night combination. In the current simulations we assume that the emissivity of a dew film has the same value of water surface emissivity. We will measure its spectral emissivity during the course of dew occurrence.

Simulation results with the statistical day/night LST algorithm and the MMD-MIN χ^2 fitting LST algorithm are shown in Fig. 7 and Table VIII. We used the similar parameters as used in the third numerical experiment and assume that each of 80 samples mixed with the vegetation sample (no. 51 in Table II) in a proportion of 25 percent. Note that the spectral reflectance data of vegetation samples (no. 50 to 62) were obtained by measurements of single leaves. According to our recent measurements and simulations with modified BRDF kernel models [Snyder and Wan, 1996(a)], the spectral reflectance of a canopy is approximately one third of the spectral reflectance of a single leaf because of volumetric effects. We have made this adjustment for the vegetation samples in this numerical experiment in order to get a better understanding of the dew effect. After this adjustment, the emissivity of all vegetation samples is close to 0.99 so that the emissivity difference between water and vegetation is negligible. Figure 7 show the error in surface temperature and the emissivity in MODIS band 20 retrieved by the night-only method. For sample 50 to sample 79, the errors in nighttime surface temperature retrieved by both the statistical and χ^2 fitting methods are within the range of $\pm 1.5\,^{\circ}$K because dew does not change the surface emissivities of vegetation, water, and ice. But dew has a significant effect on the emissivities of most rock and soil samples as shown in Fig. 2A. As indicated in Table VIII, test A is for the surface temperature and emissivities retrieved by the day/night statistical method. Because the dew effect has not been included in the statistical regression analysis, the rms and maximum errors in nighttime surface temperatures are $1.7\,^{\circ}$K and $6.6\,^{\circ}$K, respectively. In test B, only the night observation in seven MODIS bands was used to retrieve the surface temperature and emissivities by the χ^2 fit method. The maximum error in the retrieved nighttime surface temperature reduces to $5.4\,^{\circ}$K if no MMD-MIN relationship is used, and it reduces to $3.4\,^{\circ}$K and $3.1\,^{\circ}$K if one or two MMD-MIN relationships are used. The rms error in retrieved band emissivities is reduced by a factor of 2-3. Figure 7A shows the error in surface temperatures retrieved by the statistical method in test A and by the χ^2 fitting method in test B. Figure 7B shows the error in surface emissivities in band 20, ε_{20}, retrieved by the the χ^2 fitting method in test B. Although errors in the retrieved ε_{20} are still large for some rock and soil samples, these errors are smaller than the emissivity difference between dew and these samples, which is shown by open circles in Fig. 7B. This means that ε_{20} retrieved by the night-only method can be used to detect

dew for those land types which have low ε_{20} values in dry conditions. Then we can use this information in the following processing. Test C shows the simulations results retrieved by the night-only χ^2 fitting LST method for cases without night dew, the accuracies are much better than those in Test B for cases with night dew. Tests D and E show the results retrieved by the day-only χ^2 fitting method for cases with and without dew. The MMD-MIN relationships improve the retrieval accuracies slightly. The accuracies of retrieved emissivities in bands 20, 22, and 23 are poor because the solar effects cannot be corrected well by the use of only the daytime observation data. In Test F for cases with night dew, use of both daytime and nighttime data does not improve the accuracies, even with the dew emissivity for nighttime. This is because the surface emissivity may be changed significantly between daytime and nighttime. Test G is the results retrieved by the day/night χ^2 fitting method with and without the MMD-MIN relationships in cases without night dew. Use of the MMD-MIN relationships in Tests F and G improves the accuracies by only a small amount. From the simulation results for Tests A through G, we can gain the following insights into the capability of the day/night LST algorithm to deal with the dew effects: 1) dew does not affect the LST and emissivity retrieval for most of the Earth surface which is covered by water and vegetation. 2) dew do affect the retrieval for land surfaces with low emissivities in dry conditions, mainly in semi-arid and arid areas. In these areas, dew reduces the accuracies in retrieved LST and emissivities in bands 20, 22, and 23 roughly by a factor of 2, and reduces the emissivity accuracies in other bands slightly. Considering the low frequency of dew occurrence in semi-arid and arid regions, dew is not a serious problem for LST and emissivity retrieval but it makes the processing complicated slightly. We assume that the dew effect is needed to considered for one third of the global land (determined by the MODIS land-cover and NDVI products) at a frequency less than 50%. Because the dew detection process with the night-only LST mode takes less than half the computing time for the day/night LST mode, the total computing time will be increased by less than 10 percent. 3) the MMD-MIN χ^2 fitting day/night LST algorithm can be used to deal with night-only and day-only observations at lower accuracies. Surface emissivities in MODIS bands 20, 22, and 23 cannot be retrieved accurately by the day-only option in all situations (with and without dew). It is also worth noting the differences between the ASTER TES algorithm and the MODIS day/night LST algorithm: 1) the ASTER algorithm uses five bands in the spectral region 8-12 μm, the MODIS algorithm uses four bands in the spectral range 8-13.5 μm and three bands in the spectral region 3.5-4.2 μm. Two of the seven MODIS bands, bands 23 and 33, are on the edges of the atmospheric windows. They are used to adjust the boundary atmospheric temperature and the column water vapor but not for retrieval of surface temperature and emissivities per se. 2) If the atmospheric temperature and water vapor profiles recovered from the MODIS sounding channels are accurate enough ($\delta T \leq 1$ °K, the

accuracy of cwv ≤ 10%), the ASTER algorithm can retrieve surface temperature and emissivity quite accurately. But this algorithm does not have the capability to reduce the uncertainties in the ASTER atmospheric correction product (including transmission, path radiance, and downwelling irradiance) which uses the MODIS atmospheric profiles product as input. The MODIS day/night LST algorithm uses the MODIS atmospheric profiles product only as initial conditions and has some capability to reduce the uncertainties in the atmospheric profiles by the use of self consistency in the seven MODIS bands. For water surfaces and evergreen canopies with stable and known emissivities, the LST and surface emissivity retrieved by this MODIS day/night algorithm will be compared with the values retrieved by the MODIS generalized split-window LST algorithm for additional evaluation of the self consistency. 3) The ASTER algorithm can retrieve daytime and nighttime surface temperatures and emissivities independently so that its performance will not be affected by the dew occurrence in principle. The dew occurrence will affect the MODIS day/night LST algorithm for some land-cover surfaces. Therefore, its night-only option will be used first for dew detection, and then compare the retrieved ε_{20} to its daytime value retrieved previously. If there is a significant difference, this nighttime observation data should be avoided in the day/night algorithm. If this is the only nighttime observation available in one or two weeks, it can be used for day/night retrieval at a lower accuracy and it will be flagged in the QA (quality assessment) bits. 4) These two algorithm will produce LST and surface emissivities at different spatial resolutions. Comparison between the products by these two independent algorithms can provide useful information for validation.

5.3 Cloud Cover

Cloud cover is a common problem for visible and infrared remote sensing. Although the day/night LST algorithm can be used for all land surfaces, the main purpose of this algorithm is to retrieve the surface temperature and emissivity in semi-arid and arid regions where the surface emissivity varies in a wide range. The International Satellite Cloud Climatology Project (ISCCP) C2 data from 1984 to 1987 show that the world's desert regions, which result from the sub-tropical anticyclones, are areas of total cloud amount minima, less than 30% or 50% depending on the season [Drake, 1993]. From analysis of weather satellite observations, Chahine [1995] shows that the decreases in moisture and cloudiness are coupled with the increase in surface temperature over 304 °K, suggesting a positive feedback from the atmosphere perpetuating the existing desert conditions over dry and hot deserts. With EOS AM and PM platforms, the chance to have pairs of clear-sky day/night data will be increased significantly, especially in the dry areas.

6. *VALIDATION OF THE LST ALGORITHMS*

We validated the physical principle of the day/night LST method with a ground-based sun-shadow method by measuring samples of soil, sands, grass and a black aluminum plate on the roof platform of our building at UCSB on January 19th and 26th, 1996. The solar beam is blocked for half of the samples. The TIR spectrometer views the portions in sunshine and in shadow for two separate measurements and also views a diffuse reflecting gold plate in the same spots for providing information of the solar and atmospheric downwelling radiation. After calibrating the spectrometer with blackbody at three different temperatures, another two separate measurements are made. For each sample, we obtained two pairs of data for the sunshine and shadow portions, and the diffuse reflecting gold plate. A band average procedure with the spectral response functions in seven MODIS TIR bands (i.e., 20, 22, 23, 29, 31-33) is used to achieve a high signal-to-noise ratio. Radiometric calibration is made with three blackbody temperatures, spectral emissivity of the blackbody surface and the front mirror, and the temperature of the front mirror. Then we use two methods to recover the surface temperature. In the conventional method, we use the spectral emissivity curves of samples measured with the integrating sphere system. In the sun-shadow method, we make non-linear χ^2 fit of the sun-shadow data set for recovering surface temperatures in sunshine and in shadow, and the band-averaged emissivities. The LST values of samples of sand, soil, grass and black plate in sunshine and in shadow recovered by these two methods are shown in Fig. 8. Note that the mark squares represent the first method. The standard deviations are 0.4 °K and 0.1 °K, the maximum LST differences are 0.7 °K and 0.2 °K, for the LST difference in sunshine and in shadow, respectively.

We conducted a field campaign jointly with the JPL (Jet Propulsion Laboratory) ASTER team at a large flat silt playa in Railroad Valley, Nevada, on August 3rd, 1995. MAS and TIMS (Thermal Imaging Multispectral Spectrometer) data, and field measurement data of surface spectral emissivity and temperature with TIR spectrometer and broadband radiometer were collected. Temporal and spatial analysis has been made. As shown in Table IX, LST retrieved from MAS data with the generalized split-window LST algorithm at view angle (θ_v) 18.75 ° agrees with field measurement LST values within 1 °K. In this case, the LST accuracy is mainly limited by the uncertainty in its spatial variation. The MAS was calibrated with the new method [King et al., 1996]. Three field campaigns have been conducted in 1996. The first one was conducted over a snow field at the test site in Mammoth Lakes, California, on April 2nd, 1996. The second one was conducted jointly with other EOS teams at the same silt playa site in Railroad Valley, Nevada, on June 4th, 1996. The third one was conducted in the southern BOREAS test site on 14 August, 1996. MAS data and field measurement data were collected in

early afternoon and evening during the first two field campaigns. It was a perfect clear-sky day during the field campaign at the playa site on 4 June 1996. Surface temperatures were measured by three different methods: a TIR spectrometer, an infrared thermometer, and a thermistor 1mm beneath the surface. The surface temperature is also recovered from MAS data by the use of the generalized split-window and day/night LST algorithms. These results are shown in Fig. 9. Except the daytime temperature measured by the thermistor beneath the surface (it may differ from the surface temperature because of the variation in surface energy balance caused by the changing wind speed), the surface temperature values given by five methods are all within 1 °C. The band emissivities retrieved by the day/night LST method are lower than the values measured from playa samples, which were collected at the test sites, by 0.02 in bands 31-33, and 0.09 in bands 20, 22, and 23. Note the significant fluctuations in the daytime surface temperature caused by the change in wind speed.

7. COMPUTER CODING OF THE LST ALGORITHMS

Version 1 of the MODIS LST software has been submitted to the MODIS Team.

In this version of the MODIS LST code, both the generalized split-window LST algorithm and the day/night LST algorithm have been implemented. The generalized split-window LST algorithm is used to retrieve LST for pixels with known band emissivities. The band emissivities are inferred from the land-cover type based on the previous month's MODIS land-cover product. The IGBP-type 1-km global vegetation database will be used at-launch as an alternative to the MODIS land-cover data. The numerical form of the generalized split-window LST algorithm is a linear equation of the band brightness temperatures of MODIS bands 31 and 32. A built-in look-up table in steps of 0.1 °K will be used to convert the band radiance into band brightness temperature. This LST algorithm will be very efficient in the processing. We also established a database of atmospheric look-up tables for MODIS bands 20, 22, 23, 29, 31-33, for the day/night LST algorithm. The data-base obtained from accurate atmospheric radiative transfer simulations and look-up tables and interpolation methods are used in these algorithms for numerical efficiency. The bubble chart for the LST generation process is shown in Fig. 10. The LST process is working on the granule basis. Each granule covers four or more tiles. The global sinusoidal grids system is divided into a large number of tiles, each with a nominal size of 1100 km by 1100 km (10° by 10° on the equator). An internal file of intermediate data, named MOD.AM1.V1.lst_update.TILE, will be used in the process MOD_PR11 for each tile. This file stores the most updated clear-sky data for brightness temperatures in MODIS bands 20, 22, 23, 29, 31-33, atmospheric temperature and water vapor profiles at lower levels, date and

observation time, view angle, and related QA flags for both daytime and nighttime, and solar zenith angle, NDVI, condensed information of land-cover for daytime. The at-launch IGBP-type global vegetation database and NDVI will be used to distinguish pixels (class A) covered by dense vegetation, water, snow and ice from others (class B) in barren lands, including bare soils, semi-arid and arid regions. The generalized split-window LST algorithm will be applied to class A pixels for generating the level-2 LST product at 1km resolution. As doing an experiment, we used the global land-cover classification database (named VEG_CLSS) in the Global Data Sets for Land-Atmosphere Models, ISLSCP Initiative 1: 1987-1988, Volumes 1-5, which is available in CD-ROM from NASA Goddard DAAC Science Data Center. The spatial resolution of this database is 1 by 1 degree latitude/longitude. We can delineate semi-arid and arid regions which generally agree well with the dry regions defined by climatology [Trewartha and Horn, 1980].

The major steps in the LST process for each granule of 100 MODIS scan cube (1000 scan lines with 1354 1km-resolution samples each line) are described in the following.

1) input one tile of the previous quarter's land cover product and the intermediate file MOD.AM1.lst_update.TILE.

2) input N scan-lines of MODIS geolocation 1A and 1B data and level-2 MODIS products (cloud mask, atmospheric profiles, snow, NDVI) used as input to the LST process.

3) search for clear-sky pixels by the use of the MODIS cloud mask product, skip cloudy pixels.

4) find the grids covered with each clear-sky pixel, and calculate their coverages.

5) determine pixels with known band emissivities by the use of the previous quarter's land-cover product, MODIS snow cover, and NDVI products. These products can be used to identify dense vegetation (evergreen needleleaf forest, evergreen broadleaf forest, deciduous needleleaf forest, deciduous broadleaf forest, grasslands, croplands, if NDVI > 0.8), water, snow, ice. Their emissivities in bands 31 and 32 can be calculated from the coverages of these land cover types and the emissivity knowledge base. Then LST can be retrieved with the generalized split-window LST algorithm.

5') for other pixels, retrieve LST with the generalized split-window algorithm by the use of the emissivity values in bands 31 and 32 that were retrieved by the day/night algorithm in previous days. This retrieved LST needs to be compared with and may be refined by the values retrieved by the day/night algorithm later.

6) calculate and accumulate the values at each grid that will be used in the day/night LST algorithm.

7) back to (2) if the granule is not completed.

8) find new pairs of daytime and nighttime co-registered pixels

9) proceed the statistical regression approach for the day/night LST method to retrieve surface temperatures and emissivities.

10) proceed the χ^2 fit approach of the day/night LST method for pixels in which the MODIS atmospheric temperature and water vapor profiles product has high quality.

11) L3 LST quality assessment. The LST retrieved by the day/night algorithm will be compared with and may be refined or replaced by the values retrieved by the generalized split-window algorithm, especially for land cover types with high and stable emissivities in bands 31 and 32.

12) output L3 LST for the tile.

13) update and output the intermediate tile file.

14) L2 LST quality assessment.

15) output N scan-lines of L2 LST.

16) go to 1) if there is more tiles.

The value of N in 2) is determined by the memory requirement and the size of the main memory on the CPU. We use 10 as its initial value. If N equals to the total number of scan lines in the granule, step 7) will be skipped. If the computer system has enough main memory, all tiles can be processed with only one-time input of the granule files. But most likely it is not the case in the beginning of the at-launch processing.

8. OTHER ACTIVITIES

An International Land-Surface Temperature Workshop was held on September 17-19, 1996, at the University of California Santa Barbara. Jeff Dozier, Dean of the UCSB School of Environmental Science & Management welcomed the participants. Twenty five participants from USA, France, Australia and Japan attended the workshop. Twenty presentations were followed by two discussion sessions. It was a successful and productive workshop. The workshop was part of a continuing effort to maintain contact among members of the EOS community that are concerned with the improvement of LST algorithms, the definition of procedures for validation of LST, and the identification of the sources and the magnitude of measurement uncertainties. The specific goals of the Workshop were to clarify the present state of the art in LST estimation from spaceborne sensors and to identify future directions including issues requiring further research effort. A subsidiary goal was to establish a closer relationship between LST algorithm designers and the LST user community.

The new version (October 1996) of MODIS LST ATBD (algorithm theoretical basis document) was reviewed by five reviewers in November 1996 and by the EOS Review Panel on December 11, 1996. The scores given by the reviewers (2 As, 1 A-, and 2 Bs) reflect the significant improvement of the ATBD and the progress of the MODIS LST algorithms in the past two years.

REFERENCES

Adams, C. N. and G. W. Kattawar, "Radiative transfer in spherical shell atmospheres I. Rayleigh scattering," *Icarus*, vol. 35, no. 1, pp. 139-151, 1978.

Becker, F., "The impact of spectral emissivity on the measurement of land surface temperature from a satellite," *Int. J. Remote Sens.*, vol. 8, no. 10, pp. 1509-1522, 1987.

Becker, F. and Z.-L. Li, "Toward a local split window method over land surface," *Int. J. Remote Sens.*, vol. 11, no. 3, pp. 369-393, 1990.

Berk, A., L. S. Bemstein, and D. C. Robertson, "MODTRAN: A moderate resolution model for LOWTRAN 7," Rep. GL-TR-89-0122, Burlington, MA: Spectral Sciences, Inc., 1989.

Berk, A., L. S. Bemstein, and D. C. Robertson, "MODTRAN: A moderate resolution model for LOWTRAN," Rep. AFGL-TR-87-0220, Burlington, MA: Spectral Sciences, Inc., 1987.

Bevington, P. R., *Data Reduction and Error Analysis for the Physical Sciences*, New York: McGraw-Hill Book Company, 1969.

Burch, D. E. and R. L. Alt, "Continuum absorption by H_2O in the 700-1200 cm^{-1} and 2400-2800 cm^{-1} windows," Rep. AFGL-TR-84-0128, Hanscom AFB, MA: Ford Aerospace and Communication Corporate, 1984.

Chahine, M. T., "Observation of local cloud and moisture feedbacks over high ocean and desert surface temperature," *J. Geophys. Res.*, vol. 100, no. D5, pp. 8919-8927, 1995.

Chandrasekhar, S., *Radiative Transfer*, New York: Dover Publications, 1960.

Clough, S. A., F. X. Kneizys, and R. W. Davies, "Line shape and the water vapor continuum," *Atmos. Res.*, vol. 23, pp. 229-241, 1989.

Clough, S. A., "The water vapor continuum and its role in remote sensing," in *Proc. of Conference on Optical Remote Sensing of the Atmosphere, Salt Lake City, Utah*, pp. 76-78, 1995.

Clough, S. A., R. D. Worsham, W. L. Smith, H. E. Revercomb, R. O. Knuteson, G. P. Andrson, M. L. Hoke, and F. X. Kneizys, "Validation of FASCODE calculations with HIS spectral radiance measurements," in *IRS '88: Current Problems in Atmospheric Radiation*, ed. J. Lenoble and J.-F. Geleyn, pp. 376-379, Hampton, Va., USA: A. Deepak Publishing, 1989.

Clough, S. E., F. X. Kneizys, E. P. Shettle, and G. P. Anderson, "Atmospheric radiance and transmission: FASCOD2," in *Proc. of the Sixth Conference on Atmospheric Radiation, Williamsburg, VA*, pp. 141-144, Boston, MA: American Meteorological Society, 1986.

Cornette, W. M., P. K. Acharya, D. C. Robertson, and G. P. Anderson, "Moderate spectral atmospheric radiance and transmittance code (MOSART)," Rep. R-057-94(11-30), La Jolla, CA: Photon Research Associates, Inc., 1994.

Dennis, J.E. JR. and R. B. Schnabel, *Numerical Methods for Unconstrained Optimization and Nonlinear Equations,* New Jersey: Prentice-Hall, Inc., 1983.

Drake, F., "Global cloud cover and cloud water path from ISCCP C2 data," *Int. J. Climatology*, vol. 13, pp. 581-605, 1993.

Fu, Q. and K.-N. Liou, "On the correlated k-distribution method for radiative transfer in nonhomogeneous atmospheres," *J. Atmos. Sci.*, vol. 49, no. 22, pp. 2139-2156, 1992.

Gleason, M. L., S. E. Taylor, T. M. Loughin, and K. J. Koehler, "Development and validation of an empirical model to estimate the duration of dew periods," *Plant Diseases*, vol. 78, no. 10, pp. 1011-1016, 1994.

Goody, R. M. and Y. L. Yung, *Atmospheric Radiation,* New York: Oxford University Press, 1989.

Grant, W. B., "Water vapor absorption coefficients in the 8-13-μm spectral region: a critical review," *Appl. Optics*, vol. 29, no. 4, pp. 451-462, 1990.

Hook, S. J., A. R. Gabell, A. A. Green, and P. S. Kealy, "A comparison of techniques for extracting emissivity information from thermal infrared data for geological studies," *Remote Sens. Environ.*, vol. 42, pp. 123-135, 1992.

Isaacs, R. G., W-C. Wang, R. D. Worsham, and S. Goldberg, "Multiple scattering LOWTRAN and FASCODE models," *Appl. Optics*, vol. 26, pp. 1272-1281, 1987.

Janssen, L. H. J. M. and F. G. Römer, "The frequency and duration of dew occurrence over a year: model results compared with measurements," *Tellus*, vol. 43B, no. 5, pp. 408-419, 1991.

Kahle, A. B., D. P. Madura, and J. M. Soha, "Middle infrared multispectral aircraft scanner data: analysis for geological applications,," *Appl. Optics*, vol. 19, pp. 2279-2290, 1980.

Kahle, A. B., "Surface emittance, temperature, and thermal inertia derived from Thermal Infrared Multispectral Scanner (TIMS) data for Death Valley, California," *Geophysics*, vol. 52, no. 7, pp. 858-874, 1986.

Kerr, Y. H., J. P. Lagouarde, and J. Imbernon, "Accurate land surface temperature retrieval from AVHRR data with use of an improved split window algorithm," *Remote Sens. Environ.*, vol. 41, no. 2-3, pp. 197-209, 1992.

King, M. D., Y. J. Kaufman, W. P. Menzel, and D. Tanré, "Remote sensing of cloud, aerosol, and water vapor properties from the Moderate Resolution Imaging Spectrometer (MODIS)," *IEEE Trans. Geosci. Remote Sens.*, vol. 30, no. 1, pp. 2-27, 1992.

King, M. D., W. P. Menzel, P. S. Grant, J. S. Myers, G. T. Arnold, S. E. Platnick, L. E. Gumley, S. C. Tsay, C. C. Moeller, M. Fitzgerald, K. S. Brown, and F. G. Osterwisch, "Airborne scanning spectrometer for remote sensing of cloud, aerosol, water vapor and surface properties ," *J. Atmos. Ocean. Technol.*, vol. 13, pp. 777-794, 1996.

Kneizys, F. X., E. P. Shettle, L. W. Abreu, J. H. Chetwynd, G. P. Anderson, W. O. Gallery, J. E. A. Selby, and S. A. Clough, "Users Guide to LOWTRAN 7," Rep. AFGL-TR-88-0177, Bedford, MA: Air Force Geophys. Lab., 1988.

Kneizys, F. X., E. P. Shettle, W. O. Gallery, J. H. Chetwynd, L. W. Abreu, J. E. A. Selby, S. A. Clough, and R. W. Fenn, "Atmospheric Transmittance/Radiance: Computer Code LOWTRAN 6," Rep. AFGL-TR-83-0187 (NTIS AD

A137796), Bedford, MA: Air Force Geophys. Lab., 1983.

Lacis, A. A. and V. Oinas, "A description of the correlated kappa-distribution method for modeling nongray gaseous absorption, thermal emission, and multiple scattering in vertically inhomogeneous atmospheres," *J. Geophys. Res.*, vol. 96, no. D5, pp. 9027-9063, 1991.

Li, Z.-L. and F. Becker, "Feasibility of land surface temperature and emissivity determination from AVHRR data," *Remote Sens. Environ.*, vol. 43, pp. 67-85, 1993.

Ma, Q. and R. Tipping, "The detailed balance requirement and general empirical formalisms for continuum absorption," *J. Quant. Spectrosc. Radiat. Transfer*, vol. 51, pp. 751-757, 1994.

Ma, Q. and R. Tipping, "A far wing line shape theory and its application to the foreign-broadened water vapor continuum absorption .3," *J. Chem. Phys.*, vol. 97, pp. 818-828, 1992.

Majumdar, T. J. and B. B. Bhattacharya, "Simulation of thermal inertia imagery with daytime HCMM data," *Int. J. Remote Sens.*, vol. 11, no. 1, pp. 139-147, 1990.

Mannstein, H., "Surface energy budget, surface temperature and thermal inertia," in *Remote Sensing Applications in Meteorology and Climatology*, ed. R. A. Vaughan and D. Reidel, NATO ASI Ser. C: Math. Phys. Sci. Vol. 201, pp. 391-410, Dordrecht, Netherlands: A Reidel Publishing Co., 1987.

Meador, W. E. and W. R. Weaver, C. N. Cuzzi, T. P. Ackerman, and L. C. Helmle, "The delta-four-stream approximation for radiative flux transfer," *J. Atmos. Sci.*, vol. 39, no. 4, pp. 917-925, 1982.

Menzel, W. P. and J. F. W. Purdom, "Introducing GOES-I - the 1st of a new generation of geostationary operational environmental satellites," *Bull. Amer. Meteor. Soc.*, vol. 75, no. 5, pp. 757-781, 1994.

Moine, P., A. Chedin, and N. A. Scott, "Automatic classification of air mass type from satellite vertical sounding data. Application to NOAA-7 observations," *Ocean-Air Interactions*, vol. 1, pp. 95-108, 1987.

NASA,, *Heat Capacity Mapping Mission User's Guide,* 119 pp., Greenbelt, MD: NASA Goddard Space Flight Ctr., 1980.

Ottlé, C. and M. Stoll, "Effect of atmospheric absorption and surface emissivity on the determination of land temperature from infrared satellite data," *Int. J. Remote Sens.*, vol. 14, no. 10, pp. 2025-2037, 1993.

Prata, A. J., "Land surface temperatures derived from the advanced very high resolution radiometer and the along-track scanning radiometer 2. experimental results and validation of AVHRR algorithms," *J. Geophys. Res.*, vol. 99, no. D6, pp. 13025-13058, 1994.

Price, J. C., "Land surface temperature measurements from the split window channels of the NOAA-7 AVHRR," *J. Geophys. Res.*, vol. 79, pp. 5039-5044, 1984.

Price, J. C., "On the analysis of thermal infrared imagery: the limited utility of apparent thermal inertia," *Remote Sens. Environ.*, vol. 18, pp. 59-73, 1985.

Robert, R., J. Selby, and L. Biberman, "Infrared continuum absorption by atmospheric water vapor in the 8-12 micron window," *Appl. Optics*, vol. 15, pp. 2085-, 1976.

Rodgers, C. D., "Retrieval of atmospheric temperature and composition from remote measurements of thermal radiation," *Rev. Geophys. and Space Phys.*, vol. 14, no. 4, pp. 609-624, 1976.

Rothman, L. S., R. R. Gamache, R. H. Tipping, C. P. Rinsland, and and others, "The HITRAN molecular database - editions of 1991 and 1992," *J. Quant. Spectros. Radiat. Transfer*, vol. 48, no. 5-6, pp. 469-507, 1992.

Running, S. W., C. Justice, V. Salomonson, D. Hall, J. Barker, Y. Kaufman, A. Strahler, A. Huete, J.-P. Muller, V. Vanderbilt, Z. Wan, and P. Teillet, "Terrestrial remote sensing science and algorithms planned for EOS/MODIS,," *Int. J. Remote Sens.*, vol. 15, no. 17, pp. 3587-3620, 1994.

Salisbury, J. W. and D. M. D'Aria, "Emissivity of terrestrial materials in the 3-5 μm atmospheric window," *Remote Sens. Environ.*, vol. 47, pp. 345-361, 1994.

Salisbury, J. W. and D. M. D'Aria, "Emissivity of terrestrial materials in the 8-14 μm atmospheric window," *Remote Sens. Environ.*, vol. 42, pp. 83-106, 1992.

Salomonson, V., W. Barnes, P. Maymon, H. Montgomery, and H. Ostrow, "MODIS: advanced facility instrument for studies of the Earth as a system," *IEEE Trans. Geosci. Remote Sens.*, vol. 27, no. 2, pp. 145-153, 1989.

Schaaf, C. B. and A. H. Strahler, "Solar zenith angle effects on forest canopy hemispherical reflectances calculated with a geometric-optical bidirectional reflectance model," *IEEE Trans. Geosci. Remote Sens.*, vol. 31, no. 4, pp. 921-927, 1993.

Scherm, H. and A. H. C. van Bruggen, "Sensitivity of simulated dew duration to meteorological variations in different climate regions of California," *Agricul. and Forest Meteorol.*, vol. 66, pp. 229-245, 1993.

Schmugge, T. J. and J. C. André, Ed., *Land Surface Evaporation: Measurements and Parameterization*, New York: Springer-Verlag, 1991.

Sellers, P. J., F. G. Hall, G. Asrar, D. E. Strebel, and R. E. Murphy, "The first ISLSCP Field Experiment (FIFE)," *Bull. Amer. Meteorol. Soc.*, vol. 69, no. 1, pp. 22-27, 1988.

Short, N. M. and L. M. Stuart, Jr., *The Heat Capacity Mapping Mission (HCMM) Anthology*, Washington, DC: NASA, 1982.

Smith, R. C., Z. Wan, and K. S. Baker, "Ozone depletion in Antarctica: modeling its effect on solar UV irradiance under clear-sky conditions," *J. Geophys. Res.*, vol. 97, no. C5, pp. 7383-7397, 1992.

Smith, W. L., H. E. Revercomb, H.-L. Huang, and R. O. Knuteson, "Vertical sounding capabilities with high spectral resolution atmospheric radiation measurements - a demonstration with the High resolution Interferometer Sounder (HIS)," in *High Spectral Resolution Infrared Remote Sensing for Earth's Weather and Climate Studies*, ed. A. Chedin, M. T. Chahine, and N. A. Scott, pp. 131-146, Berlin, Germany: Springer-Verlog, 1993.

Smith, W. L., H. M. Woolf, and A. J. Schriener, "Simultaneous retrieval of surface and atmospheric parameters: a physical and analytically direct approach," in *Advances in Remote Sensing Retrieval Methods*, ed. A. Deepak, H. E. Fleming, and M. T. Chahine, pp. 221-232, Hampton, Va., USA: A. Deepak Publishing, 1985.

Snyder, W. and Z. Wan, "Adaptation of kernel BRDF models to predict spectral reflectance and emissivity in the thermal infrared," *IEEE Trans. Geosci. Remote Sens.*, revised 1996(a).

Snyder, W. and Z. Wan, "Surface temperature correction for active infrared reflectance measurements of natural materials," *Appl. Optics*, vol. 35, no. 13, pp. 2216-2220, 1996(b).

Snyder, W., Z. Wan, Y. Zhang, and Y.-Z. Feng, "Thermal infrared (3-14 μm) bidirectional reflectance measurements of sands and soils," *Remote Sens. Environ.*, in press 1996(c).

Sobrino, J. A., C. Coll, and V. Caselles, "Atmospheric corrections for land surface temperature using AVHRR channel 4 and 5," *Remote Sens. Environ.*, vol. 38, no. 1, pp. 19-34, 1991.

Stamnes, K. and P. Conklin, "A new multi-layer discrete ordinate approach to radiative transfer in vertically inhomogeneous atmospheres," *J. Quant. Spectrosc. Radiat. Transfer*, vol. 31, pp. 273-282, 1984.

Sutton, J. C., T. J. Gillespie, and P. D. Hilebrand, "Monitoring weather factors in relation to plant disease of dew periods," *Plant Disease*, vol. 68, no. 1, pp. 78-84, 1984.

Tanré, D., C. Deroo, A. Deleffe, M. Herman, and J. J. Morcrette, "Description of a computer code to simulate the satellite signal in the solar spectrum: the 5S code," *Int. J. Remote Sens.*, vol. 11, no. 4, pp. 659-668, 1990.

Thériault, J.-M., P. L. Roney, D. St.-Germain, H. E. Revercomb, R. O. Knuteson, and W. L. Smith, "Analysis of the FASCODE model and its H_2O continuum based on long-path atmospheric transmission measurements in the 4.5-11.5μm region," *Appl. Optics*, vol. 33, no. 3, pp. 323-333, 1994.

Trewartha, G. T. and L. H. Horn, in *An Introduction To Climate*, New York: McGraw-Hill Book Company, 1980.

Varanasi, P., "On the nature of the infrared spectrum of water vapor between 8 and 14 μm," *J. Quant. Spectros. Radiat. Transfer*, vol. 40, no. 3, pp. 169-175, 1988.

Vidal, A., "Atmospheric and emissivity correction of land surface temperature measured from satellite using ground measurements or satellite data," *Int. J. Remote Sens.*, vol. 12, no. 12, pp. 2449-2460, 1991.

Vukovich, F. M., "A comparison of surface temperature derived from HCMM infrared measurements with field data," *Remote Sens. Environ.*, vol. 15, pp. 63-76, 1984.

Wan, Z. and J. Dozier, "Effects of the atmosphere and surface emissivity on the thermal infrared spectral signature measured from MODIS-N," *Proc. IGARSS '90*, pp. 189-192, 1990.

Wan, Z. and J. Dozier, "A generalized split-window algorithm for retrieving land-surface temperature from space," *IEEE Trans. Geosci. Remote Sens.*, vol. 34, no. 4, pp. 892-905, 1996.

Wan, Z. and J. Dozier, "Land-surface temperature measurement from space: physical principles and inverse modeling," *IEEE Trans. Geosci. Remote Sens.*, vol. 27, no. 3, pp. 268-278, 1989.

Wan, Z. and Z.-L. Li, "A physics-based algorithm for retrieving land-surface emissivity and temperature from EOS/MODIS data," *IEEE Trans. Geosci. Remote Sens.*, accepted 1996.

Wang, J., G. P. Anderson, H. E. Revercomb, and R. O. Knuteson, "Validation of FASCOD3 and MODTRAN3: comparison of model calculations with ground-based and airborne interferometer observations under clear-sky conditions," *Appl. Optics*, accepted 1996.

Westwater, E. R., J. B. Snider, J. H. Churnside, and J. A. Shaw, "Ground based microwave and infrared radiance observations during Probe," in *Proc. of the Eighth Conference on Atmospheric Radiation, AMS, Nashville, TN*, pp. 272-275, 1994.

Wiscombe, W. J., "The delta-M method: rapid yet accurate radiative flux calculations for strong asymmetric phase functions," *J. Atmos. Sci.*, vol. 34, pp. 1408-1422, 1977.

Wiscombe, W. J. and J. W. Evans, "Exponential-sum fitting of radiative transmission functions," *J. Comput. Phys.*, vol. 24, no. 4, pp. 416-444, 1977.

Wiscombe, W. J., "Extension of the doubling method to inhomogeneous sources," *J. Quant. Spectros. Radiat. Transfer*, vol. 16, no. 6, pp. 477-486, 1976.

Zangvil, A., "Six years of dew observations in the Negev Desert, Israel," *Journal of Arid Environ.*, vol. 32, pp. 361-371, 1996.

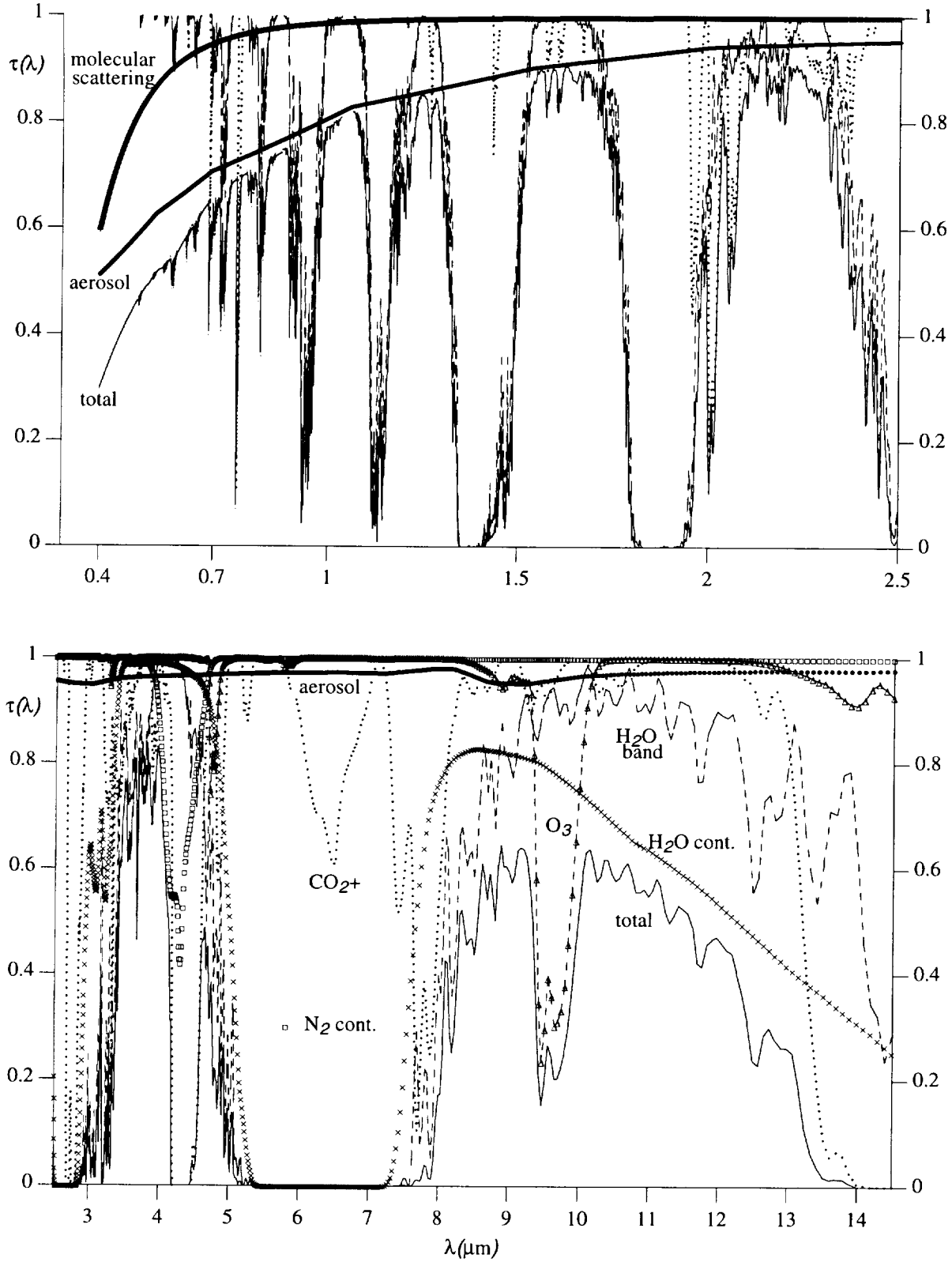

Fig. 1, Atmospheric transmissions at view angle 45° in mid-latitude summer condition (cwv = 2.9cm, vis. = 23km).

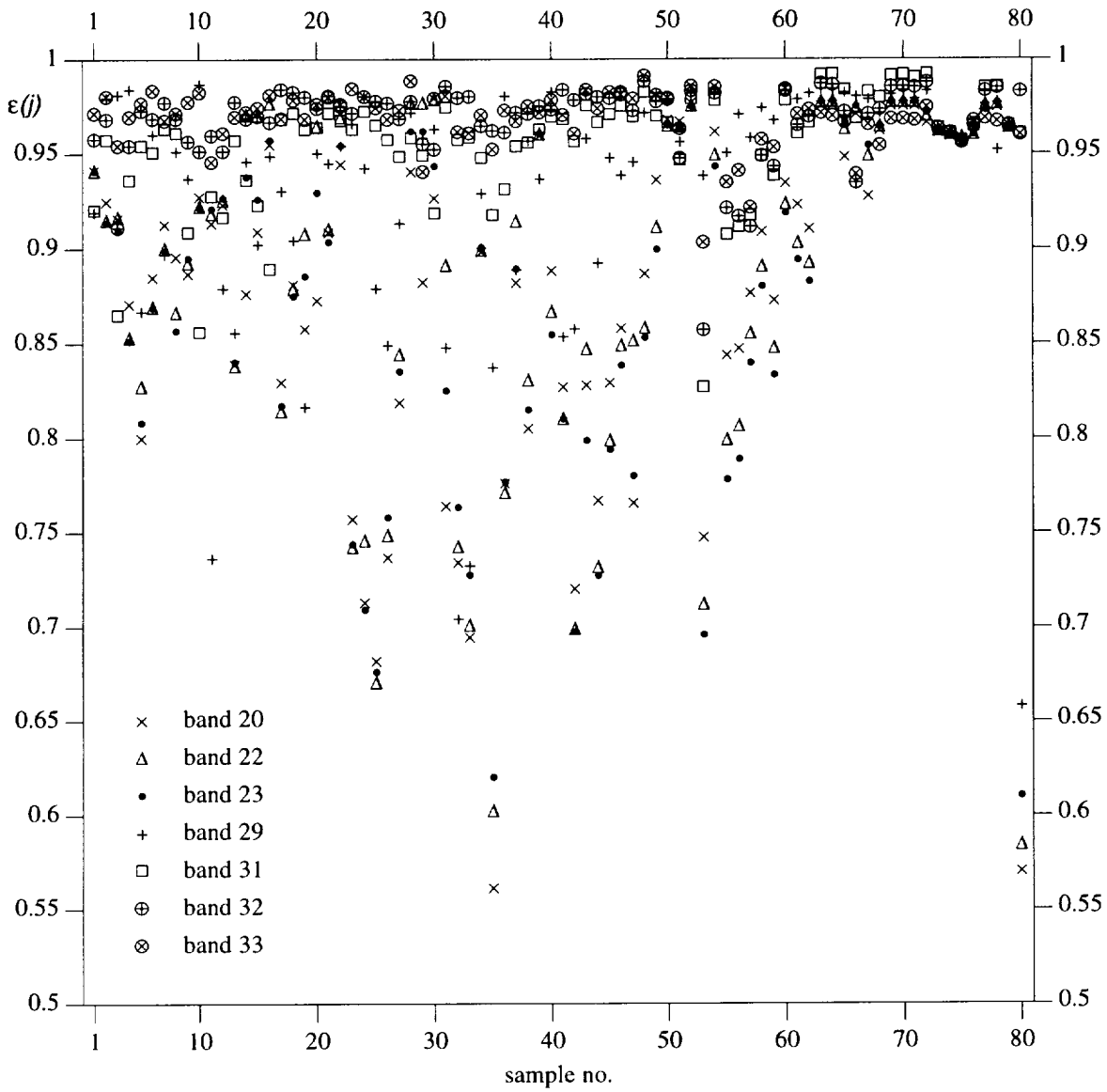

Fig. 2, Band-averaged emissivities in MODIS bands 20, 22, 23, 29, 31-33 versus samples in Table II.

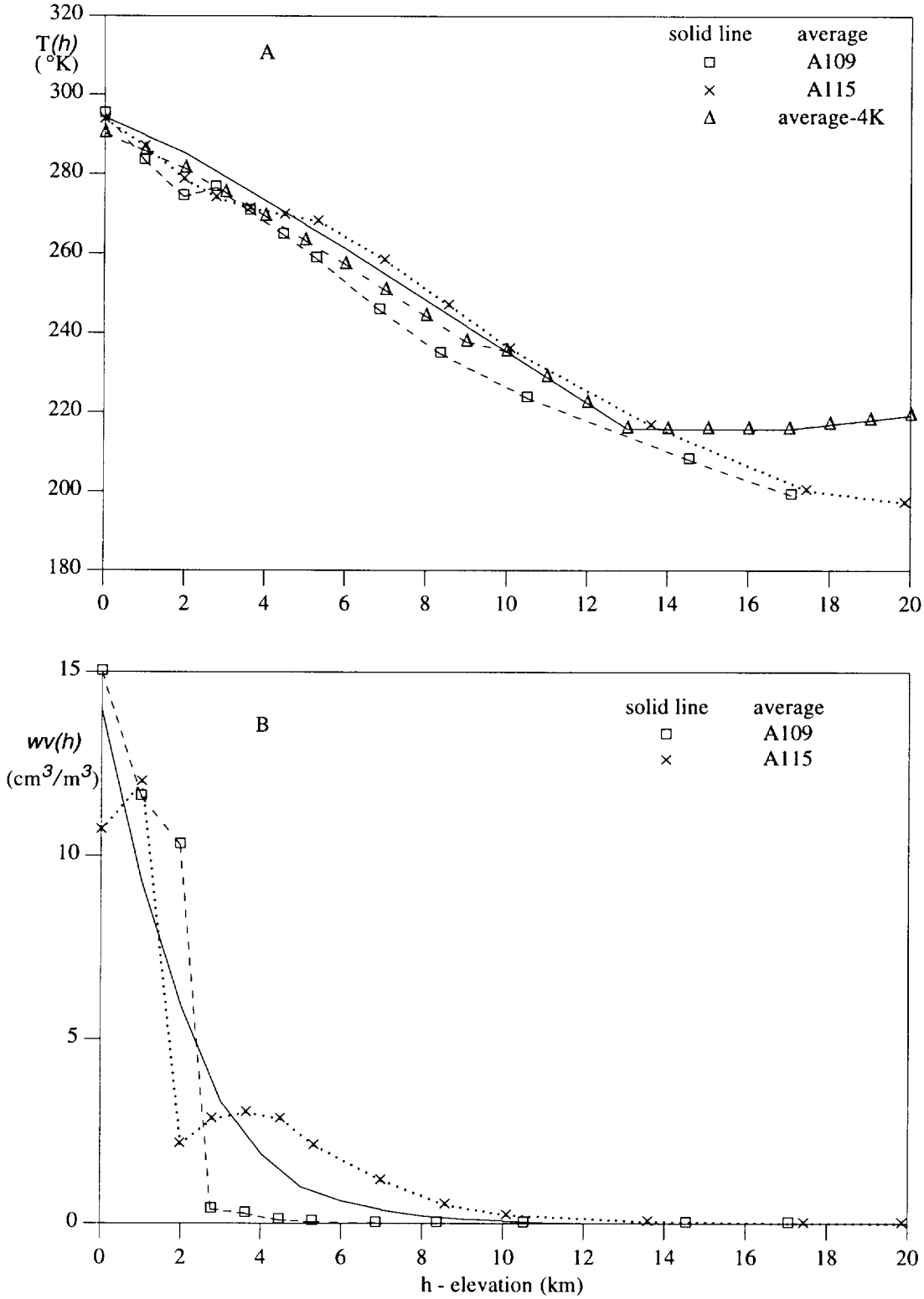

Fig. 3, Atmospheric temperature profiles (A) and water vapor profiles (B) in mid-latitude summer.

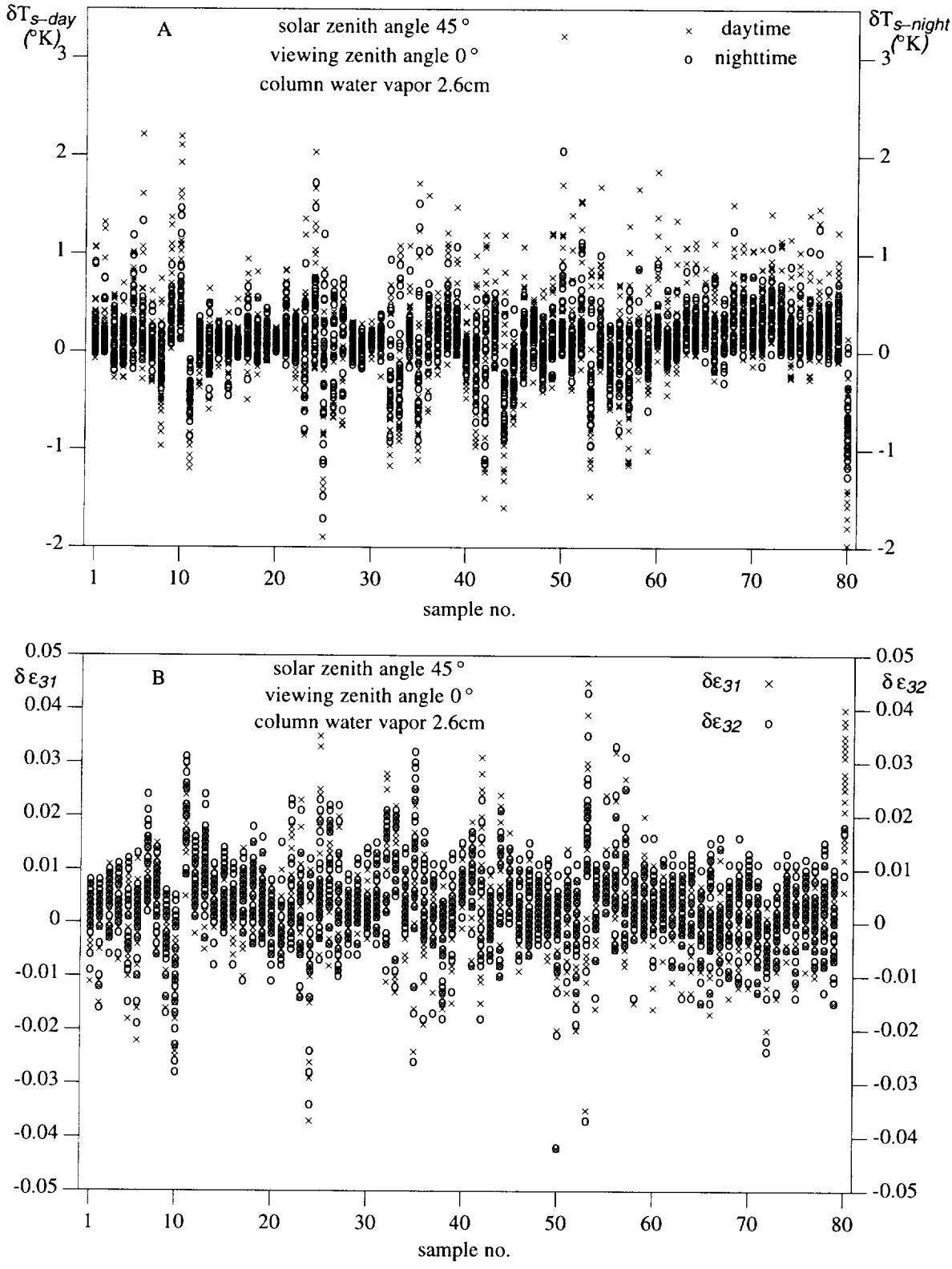

Fig. 4, Errors in surface temperatures (A) and emissivities (B) retrieved by the χ^2 fit method.

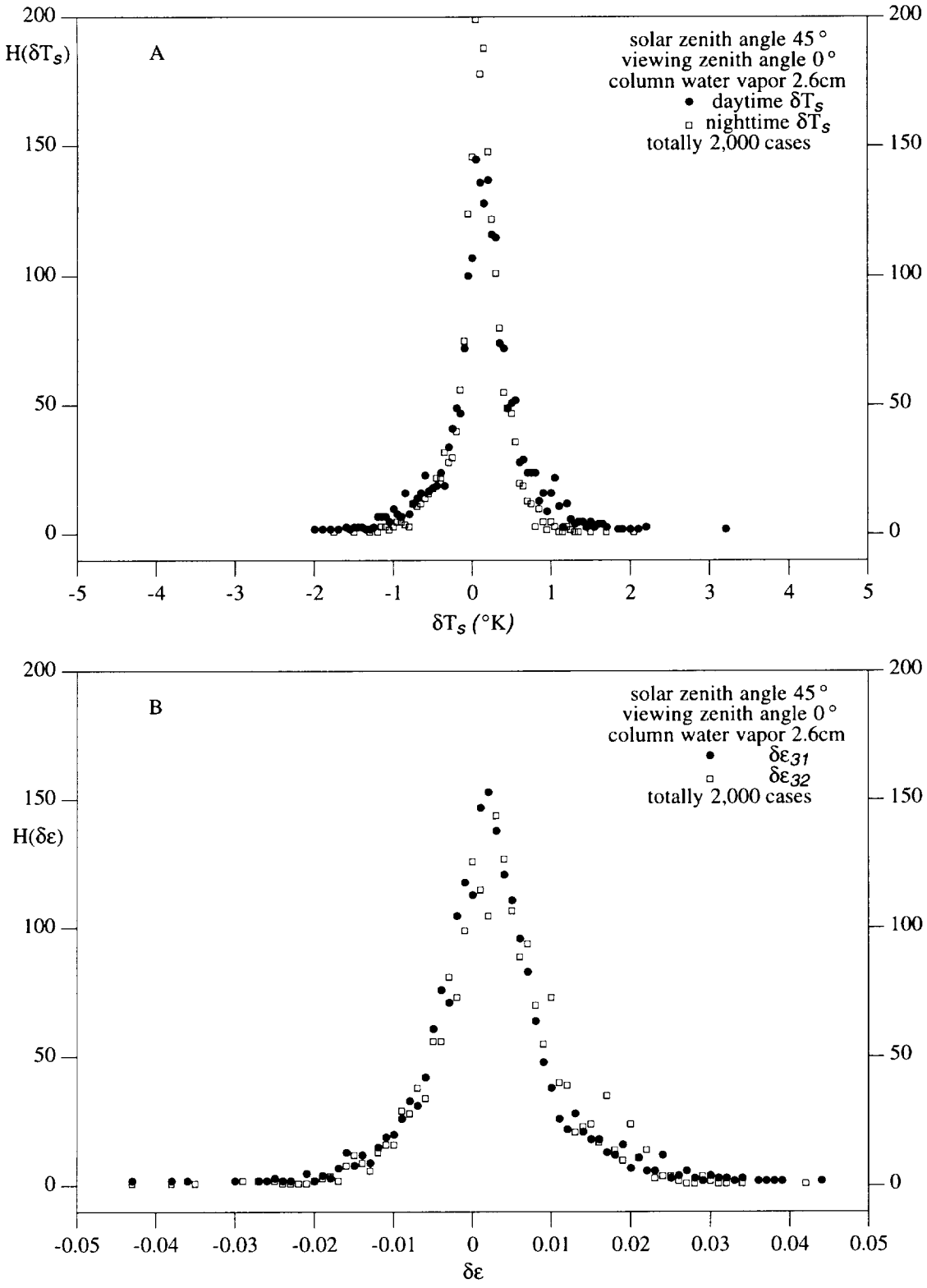

Fig. 5, Histogram of errors in surface temperatures (A) and emissivities (B) retrieved by the χ^2 fit method.

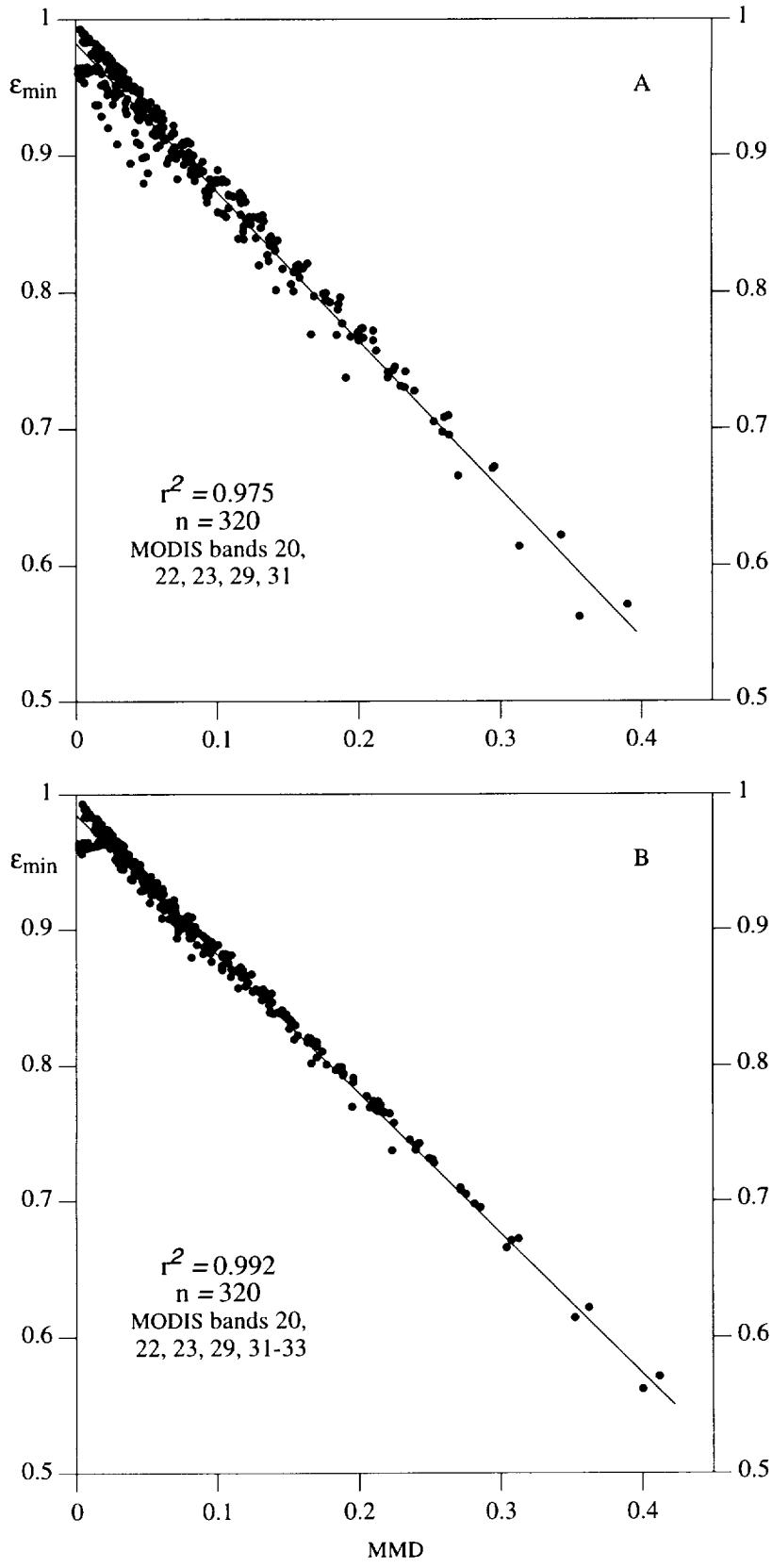

Figure 6. The empirical ε_{min} vs MMD relationships in five MODIS bands (A) and seven MODIS bands (B).

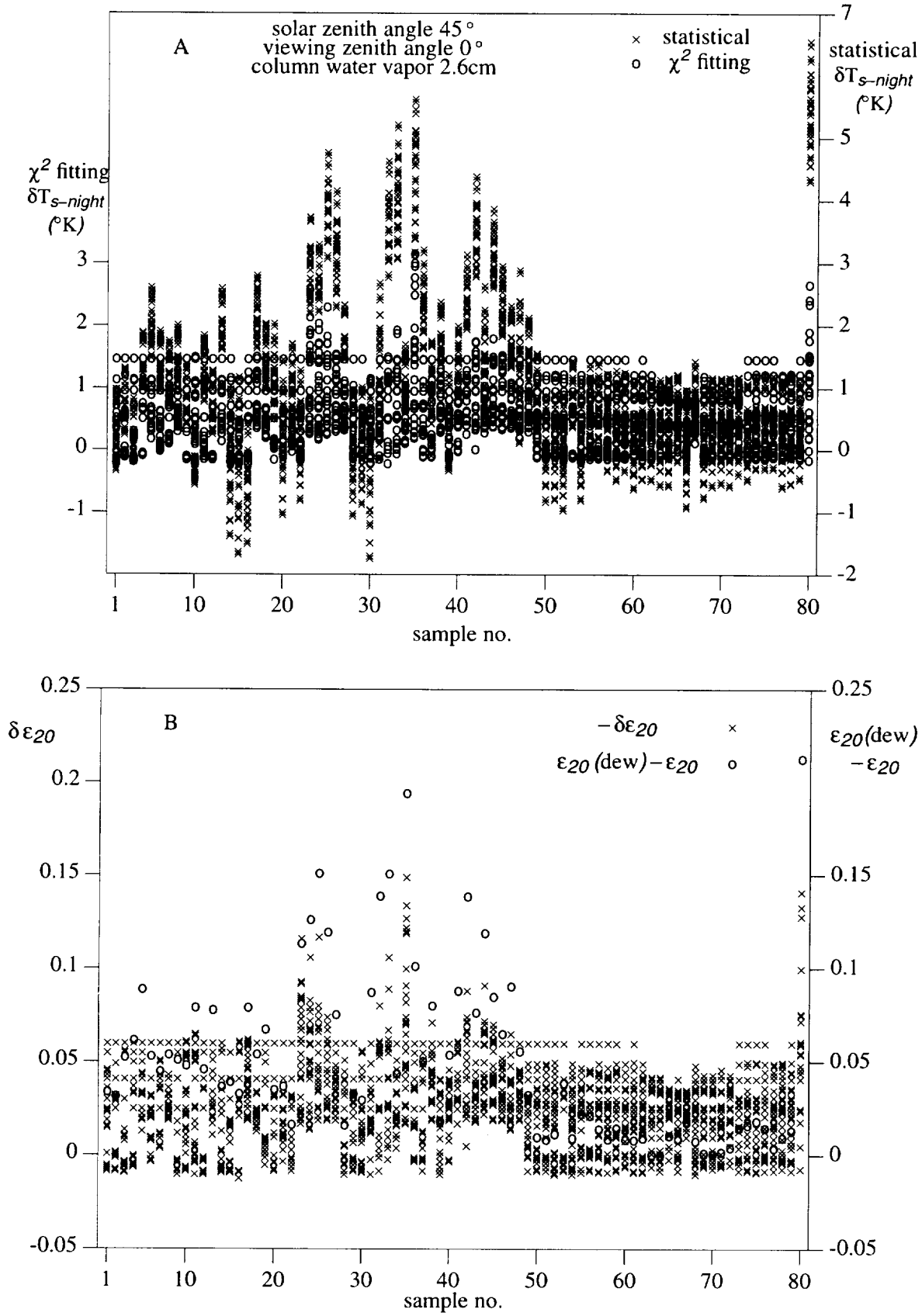

Figure 7, Errors in surface temperatures (A) and ε_{20} (B) retrieved in case of night dew.

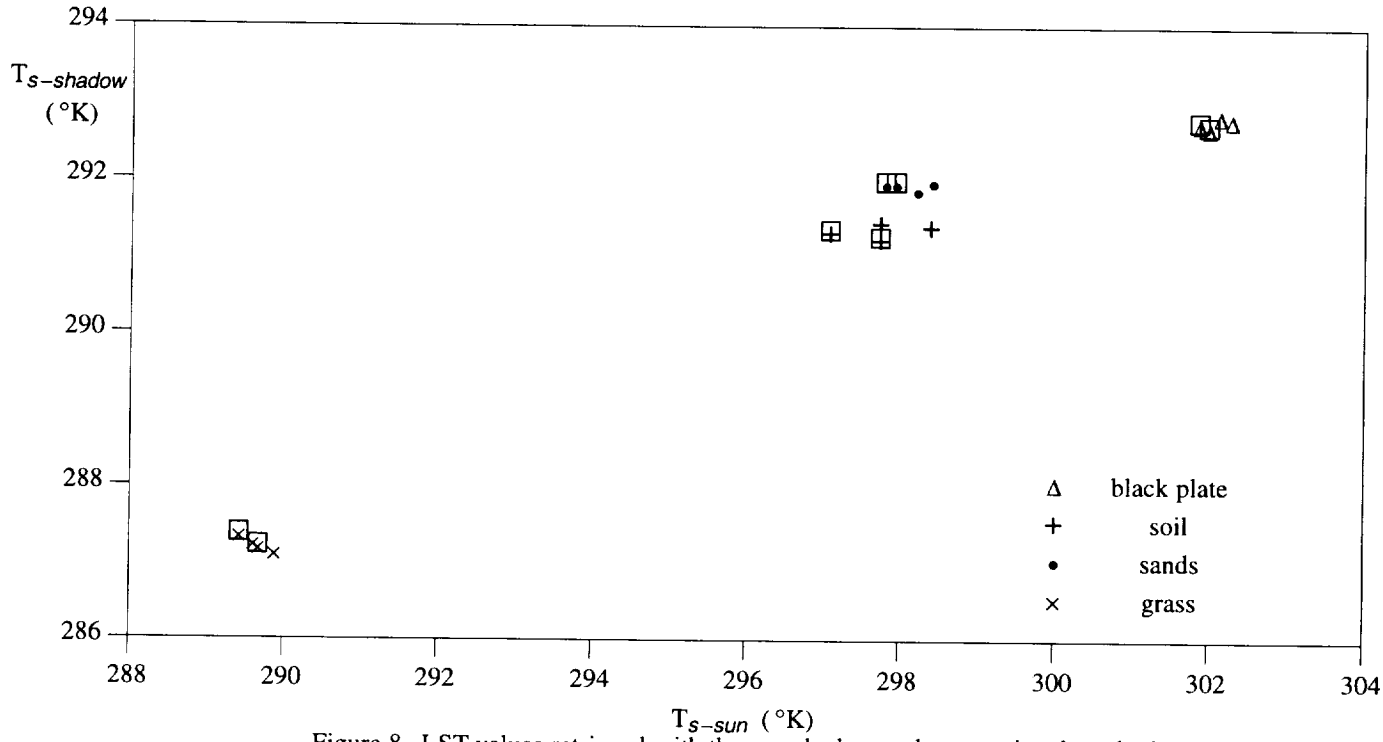

Figure 8, LST values retrieved with the sun-shadow and conventional methods.

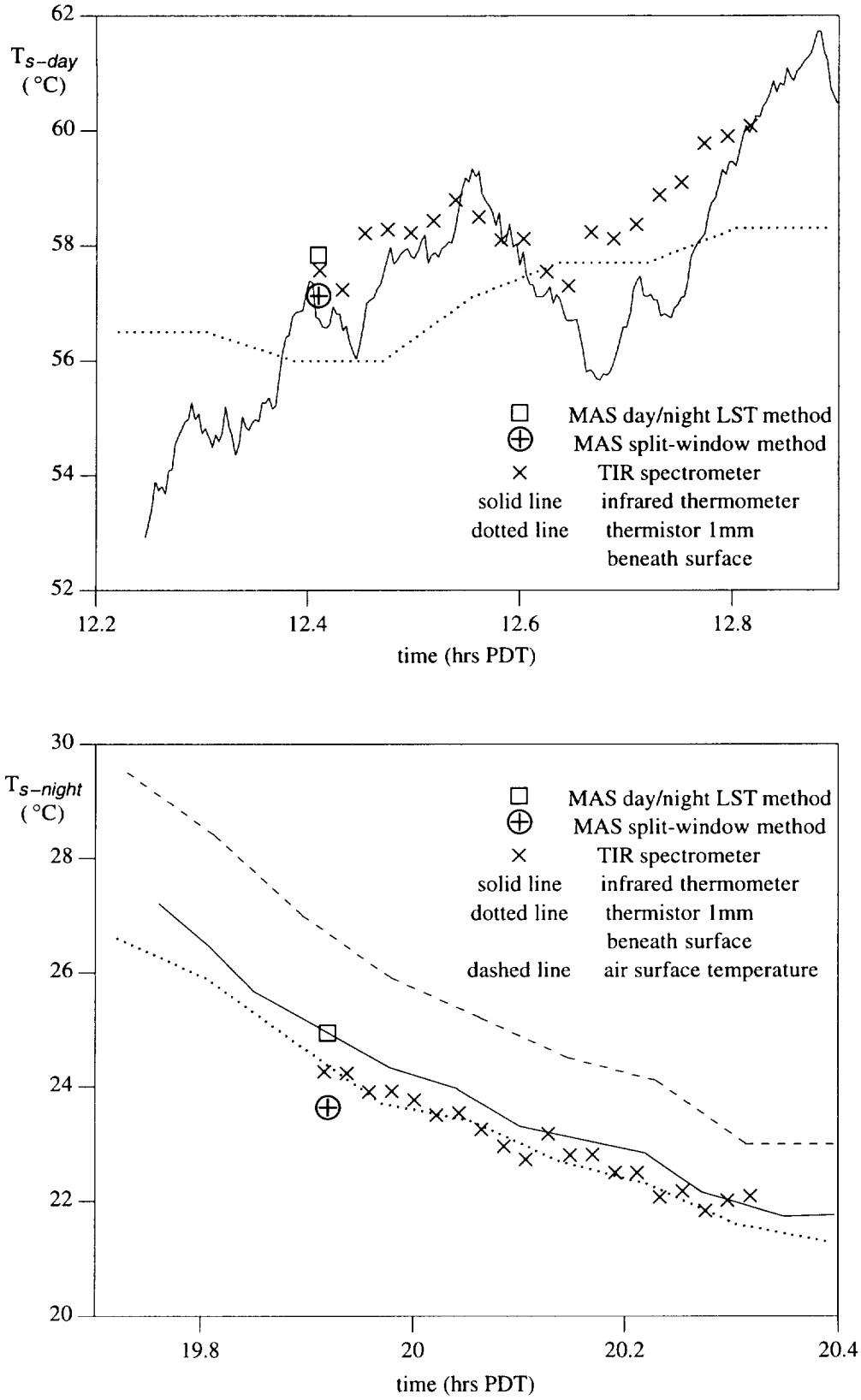

Figure 9, LST measured at a playa site in Railroad Valley, ND, on 4 June, 1996.

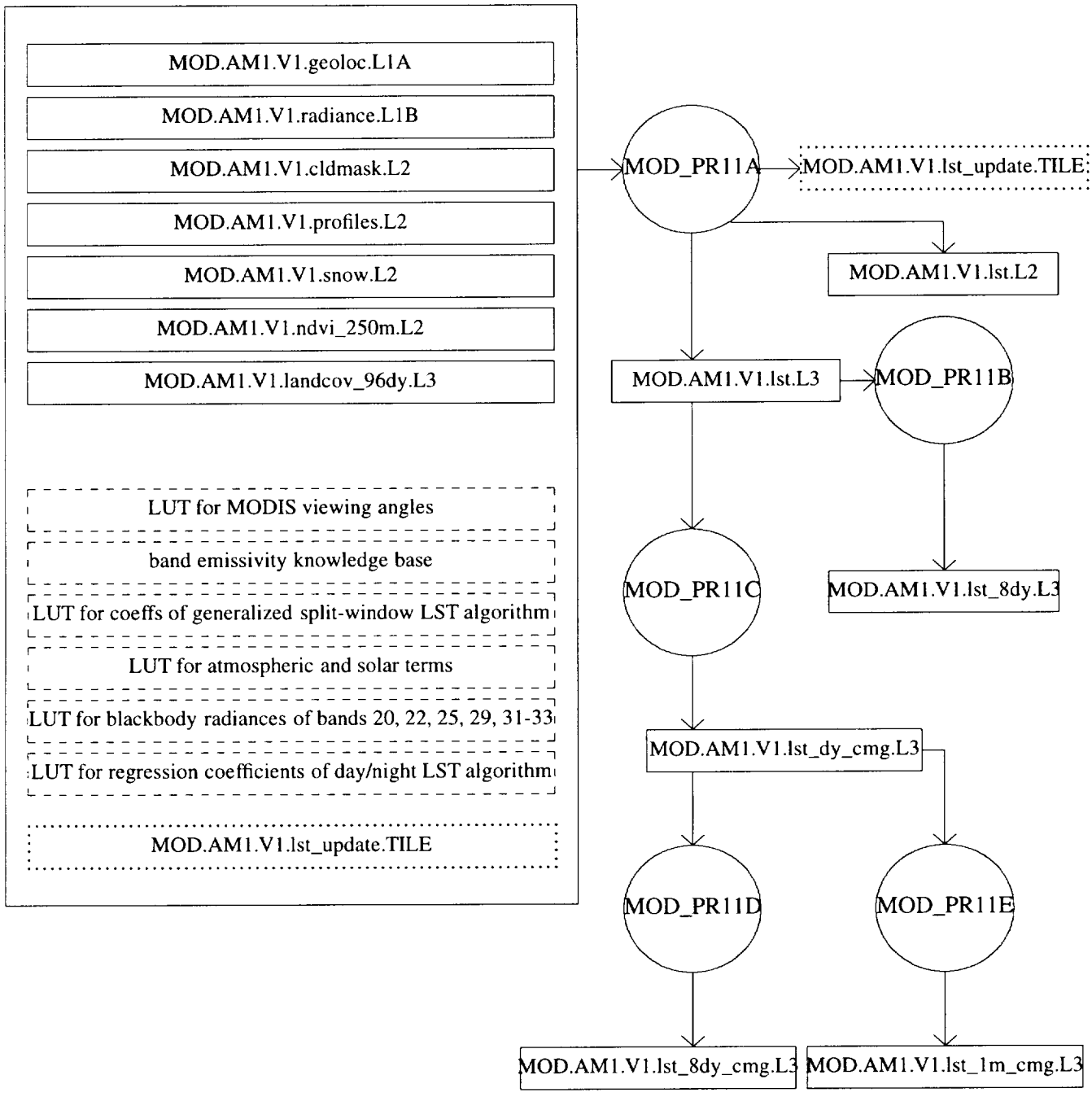

designed by Z. Wan 10/19/96

Figure 10. Bubble chart for MOD_PR11

TABLE I. Specifications of the EOS MODIS bands.

band	bandwidth (nm)	IFOV	primary use	band	bandwidth (μm)	IFOV	$NE\Delta T$ (°K)	primary use
1	620- 670	250m	L	20	3.660-3.840	1km	0.05	O, L
2	841- 876	250m	A, L	21	3.929-3.989	1km		fire, volcano
3	459- 479	500m	L	22	3.929-3.989	1km	0.07	A, L
4	545- 565	500m	L	23	4.020-4.080	1km	0.07	A, L
5	1230-1250	500m	L	24	4.433-4.498	1km	0.25	A
6	1628-1652	500m	A, L	25	4.482-4.549	1km	0.25	A
7	2105-2155	500m	A, L	27	6.535-6.895	1km	0.25	A
8	405- 420	1km	O	28	7.175-7.475	1km	0.25	A
9	438- 448	1km	O	29	8.400-8.700	1km	0.05	L
10	483- 493	1km	O	30	9.580-9.880	1km	0.25	ozone
11	526- 536	1km	O	31	10.780-11.280	1km	0.05	A, L
12	546- 556	1km	O	32	11.770-12.270	1km	0.05	A, L
13	662- 672	1km	O	33	13.185-13.485	1km	0.25	A, L
14	673- 683	1km	O	34	13.485-13.785	1km	0.25	A
15	743- 753	1km	A	35	13.785-14.085	1km	0.25	A
16	862- 877	1km	A	36	14.085-14.385	1km	0.35	A
17	890- 920	1km	A					
18	931- 941	1km	A					
19	915- 965	1km	A					
26	1360-1390	1km	cirrus					

Note: A - atmospheric studies; L - land studies; O - ocean studies. Ref: MODIS Level 1B Algorithm Theoretical Basis Document, 1995, NASA/GSFC, Greenbelt, MD.

TABLE II. List of terrestrial material samples.

sample no.	sample name	type of material	sample no.	sample name	type of material
1	basalt.f	fresh rough surface	41	0135	soil (Entisols)
2	basalt.v	desert vanish coated rock	42	0145	soil (Ultisols)
3	ijolite.f	fresh rough surface	43	0211	soil (Molisols)
4	ijolite.v	desert vanish coated rock	44	0219	soil (Alfisols)
5	rhyolite.f	fresh rough surface	45	0226	soil (Inceptisols)
6	rhyolite.v	desert vanish coated rock	46	0475	soil (Vertisols)
7	crustose.10	lichens coated rock	47	1530	soil (Aridisols)
8	crustose.65	lichens coated rock	48	4717	soil (Oxisols)
9	basalt.h7	igneous rock	49	foliose.1	veg., lichens
10	dunite.h1	igneous rock	50	indiangr.ass	veg., green foliage
11	granite.h1	igneous rock	51	redoak	veg., green foliage
12	syenite.h1	igneous rock	52	white.ine	veg., green foliage
13	greywack.eh1	sedimentary rock	53	senbeech	veg., senescent foliage
14	limeston.eh1	sedimentary rock	54	senpine	veg., senescent foliage
15	limeston.eh2	sedimentary rock	55	senredoa.kh1	veg., senescent foliage
16	limeston.eh3	sedimentary rock	56	senryegr.ass	veg., senescent foliage
17	sandton.eh1	sedimentary rock	57	oakbark.1	veg., tree bark
18	sandton.eh2	sedimentary rock	58	pinebark.1	veg., tree bark
19	sandton.eh4	sedimentary rock	59	ypoplarb.ark	veg., senescent foliage
20	shale.h3	sedimentary rock	60	conifer.ous	veg. decomposing litter
21	shale.h5	sedimentary rock	61	decidu.ous	veg. decomposing litter
22	shale.h6	sedimentary rock	62	wood	veg. decomposing litter
23	siltston.eh1	sedimentary rock	63	seawater	water
24	siltston.eh2	sedimentary rock	64	distwa.ter	water
25	gneiss.h1a	metamorphic rock	65	distice1.00g	ice
26	gneiss.h3a	metamorphic rock	66	distices.moo	ice
27	gneiss.h4	metamorphic rock	67	seaice.10.ogr	ice
28	marble.h2	metamorphic rock	68	seaicesm.oot	ice
29	marble.h3	metamorphic rock	69	qtzwater.23	suspended sediments
30	marble.h4	metamorphic rock	70	qtzwater.64	suspended sediments
31	quartzit.eh1	metamorphic rock	71	qtzwater.7	suspended sediments
32	quartzit.eh4	metamorphic rock	72	foam	water coatings
33	quartzit.eh6	metamorphic rock	73	oil15465	water coatings
34	schist.h3a	metamorphic rock	74	oil34792	water coatings
35	schist.h6a	metamorphic rock	75	oil39076	water coatings
36	schist.h7	metamorphic rock	76	oil42667	water coatings
37	slate.h1a	metamorphic rock	77	soilfl.oat	water coatings
38	slate.h2a	metamorphic rock	78	qtzfloat	water coatings
39	slate.h3	metamorphic rock	79	oil35473	water coatings
40	0127	soil (Spodosols)	80	qtz.hem	quartz

TABLE III. The standard deviations of errors in surface temperature and emissivities retrieved with two approaches of the day/night LST algorithm.

atmospheric profile	δT_{s-day} (°K)	$\delta T_{s-night}$ (°K)	$\delta\varepsilon_{20}$	$\delta\varepsilon_{22}$	$\delta\varepsilon_{23}$	$\delta\varepsilon_{29}$	$\delta\varepsilon_{31}$	$\delta\varepsilon_{32}$	$\delta\varepsilon_{33}$
			with the statistical regression approach						
average	0.91	0.73	0.021	0.025	0.027	0.013	0.012	0.014	0.012
A109	0.82	0.75	0.026	0.024	0.027	0.032	0.013	0.018	0.014
A115	1.18	0.73	0.021	0.027	0.033	0.015	0.013	0.016	0.013
average-4K	0.94	0.64	0.019	0.022	0.024	0.013	0.013	0.014	0.013
			with the χ^2 fit approach						
average	0.51	0.36	0.015	0.014	0.016	0.008	0.009	0.009	0.012
A109	2.13	1.91	0.057	0.068	0.076	0.030	0.036	0.043	0.014
A115	0.97	0.58	0.028	0.024	0.032	0.023	0.017	0.020	0.013
average-4K	0.45	0.32	0.014	0.013	0.015	0.008	0.009	0.009	0.013

TABLE IV. The RMS errors in surface temperature and emissivities retrieved with the χ^2 fit approach of the day/night LST algorithm in the sensitivity study on assumptions of surface optical properties in conditions of $T_{a-day}=298.2$°K, $T_{a-night}=290.2$°K, cwv $=2.6$cm, $\alpha=1.0$, NEΔT $=0.05$–0.12°K, and systematic calibration error = 0.5%.

test no.	test conditions	δT_{s-day} (°K)	$\delta T_{s-night}$ (°K)	$\delta\varepsilon_{31}$ (daytime)	$\delta\varepsilon_{32}$ (daytime)
C1	$\varepsilon_n(j)=\varepsilon_d(j)$ $f_r(20)=f_r(22)=f_r(23)$ Lambertian surface	0.51	0.36	0.009	0.009
C2	$\varepsilon_n(j)=\varepsilon_d(j)+0.01$	0.75	0.55	0.013	0.013
C3	$\varepsilon_n(j)=\varepsilon_d(j)+0.1\,(1-\varepsilon_d)$	0.51	0.41	0.009	0.009
C4	$f_r(22)=0.95\,f_r(23)$, $f_r(20)=0.90\,f_r(23)$	0.71	0.58	0.012	0.011
C5	$f_r(20)=1.10\,f_r(23)$, $f_r(22)=1.05\,f_r(23)$	0.68	0.60	0.011	0.011
C6	non-Lambertian surface (80%)	0.61	0.43	0.011	0.010
C7	non-Lambertian surface (120%)	0.58	0.41	0.010	0.010

TABLE V. The dependences of standard deviations (δT_s) and maximum errors (ΔT_s) in surface emissivities and temperatures retrieved with the χ^2 fit approach of the day/night LST algorithm on NEΔT and calibration errors.

test no.	NEΔT (°K)	calibration errors (%)	δT_{s-day} (°K)	$\delta T_{s-night}$ (°K)	ΔT_{s-day} (°K)	$\Delta T_{s-night}$ (°K)	$\delta\varepsilon_{31}$	$\delta\varepsilon_{32}$
D1	0.05,0.07,0.07,0.05,0.05,0.05,0.12	0.00	0.41	0.31	3.3	2.6	0.007	0.007
D2	0.05,0.07,0.07,0.05,0.05,0.05,0.12	0.50	0.51	0.36	3.2	2.1	0.009	0.009
D3	0.10,0.14,0.14,0.10,0.10,0.10,0.25	0.50	0.69	0.49	3.7	2.2	0.011	0.012
D4	0.05,0.07,0.07,0.05,0.05,0.05,0.12	0.75	0.58	0.40	3.3	2.1	0.010	0.011
D5	0.05,0.07,0.07,0.05,0.05,0.05,0.12	1.00	0.66	0.45	4.4	2.5	0.012	0.012

TABLE VI. Comparison between HCMM and MODIS TIR channels.

specification	HCMM	MODIS
orbital altitude	620km	705km
resolution	0.6km at nadir	1km at nadir
swath width	716km	2330km
spectral range	10.5-12.5 μm	3.5-14.5 μm
number of TIR channels	1	16
NEΔT	0.4 °K	0.05 °K for surface channels 0.25 °K for sounding channels
quantization	8 bits from analog data	12 bits
positioning error	≈ 3km	< 200m
spatial coverage	direct broadcast to ground stations	gloabl
launch date	April 1978	June 1998
life time	17 months	5 years

TABLE VII. The sensitivity of surface emissivities and temperature retrieved by the χ^2 fit day/night LST algorithm to uncertainties in day/night registration. The proportion of vegetation within a mixed pixel in daytime differs from that in nighttime because of mis-registration.

P (veg)		rms errors					maximum errors				
day	night	δT_{s-d} (°K)	δT_{s-n} (°K)	$\delta\varepsilon_{20}$	$\delta\varepsilon_{31}$	$\delta\varepsilon_{32}$	ΔT_{s-d} (°K)	ΔT_{s-n} (°K)	$\Delta\varepsilon_{20}$	$\Delta\varepsilon_{31}$	$\Delta\varepsilon_{32}$
		$T_{s-d}(veg) - T_{s-d}(\text{background}) = -4$°K									
0.5	0.5	0.35	0.24	0.011	0.007	0.008	3.1	1.5	0.090	0.041	0.040
0.5	0.45	0.35	0.25	0.012	0.008	0.009	1.8	1.2	0.059	0.029	0.035
0.5	0.4	0.37	0.29	0.014	0.008	0.010	1.8	2.2	0.092	0.035	0.041
0.5	0.35	0.44	0.36	0.016	0.010	0.012	2.6	3.4	0.130	0.060	0.060
0.5	0.3	0.46	0.41	0.018	0.011	0.014	2.9	3.5	0.145	0.074	0.078
0.5	0.25	0.56	0.51	0.022	0.013	0.017	4.2	4.5	0.182	0.086	0.081
0.5	0.2	0.61	0.57	0.023	0.015	0.018	4.1	3.4	0.185	0.144	0.101
		$T_{s-d}(veg) - T_{s-d}(\text{background}) = 0$°K									
0.5	0.5	0.36	0.26	0.012	0.007	0.009	2.3	1.5	0.068	0.031	0.037
0.5	0.45	0.38	0.27	0.013	0.008	0.010	2.1	1.5	0.068	0.037	0.037
0.5	0.4	0.38	0.30	0.014	0.009	0.011	1.8	1.9	0.082	0.036	0.038
0.5	0.35	0.43	0.36	0.016	0.010	0.013	2.6	2.8	0.109	0.047	0.048
0.5	0.3	0.46	0.44	0.019	0.012	0.015	2.9	4.7	0.183	0.083	0.074
0.5	0.25	0.52	0.51	0.021	0.013	0.017	3.7	3.6	0.171	0.068	0.077
0.5	0.2	0.58	0.59	0.023	0.015	0.019	4.4	4.3	0.150	0.185	0.091
		$T_{s-d}(veg) - T_{s-d}(\text{background}) = 4$°K									
0.5	0.5	0.39	0.25	0.011	0.007	0.009	3.2	1.5	0.088	0.037	0.037
0.5	0.45	0.40	0.26	0.012	0.008	0.010	2.4	1.4	0.069	0.033	0.037
0.5	0.4	0.45	0.32	0.014	0.009	0.012	2.6	2.3	0.096	0.039	0.046
0.5	0.35	0.50	0.38	0.016	0.011	0.014	2.9	3.3	0.128	0.059	0.059
0.5	0.3	0.57	0.45	0.019	0.012	0.016	4.0	4.5	0.178	0.083	0.068
0.5	0.25	0.65	0.54	0.021	0.014	0.018	4.7	4.3	0.163	0.072	0.062
0.5	0.2	0.73	0.62	0.024	0.015	0.020	5.3	3.9	0.182	0.063	0.068

TABLE VIII. The standard deviation (δ) and maximum (Δ) errors in surface temperature and emissivities retrieved with the statistical and the MMD-MIN χ^2-fitting LST algorithms in cases with and without night dew.

test	number of MMD-MIN relations used	δT_{s-day} (ΔT_{s-day} (°K)	$\delta T_{s-night}$ $\Delta T_{s-night}$	$\delta\varepsilon_{20}$ $\Delta\varepsilon_{20}$	$\delta\varepsilon_{22}$ $\Delta\varepsilon_{22}$	$\delta\varepsilon_{23}$ $\Delta\varepsilon_{23}$	$\delta\varepsilon_{29}$ $\Delta\varepsilon_{29}$	$\delta\varepsilon_{31}$ $\Delta\varepsilon_{31}$	$\delta\varepsilon_{32}$ $\Delta\varepsilon_{32}$	$\delta\varepsilon_{33}$ $\Delta\varepsilon_{33}$)
A		day/night statistical LST method for cases with night dew (including daytime ε's only)								
	0	0.87	1.71	0.026	0.029	0.026	0.023	0.012	0.013	0.014
		(3.63	6.56	0.140	0.132	0.097	0.113	0.045	0.052	0.040)
B		night-only χ^2-fitting LST method for cases with unknown night dew (retrieving dew ε's)								
	0		1.49	0.070	0.066	0.071	0.037	0.033	0.033	0.007
			(5.37	0.221	0.204	0.214	0.123	0.109	0.116	0.037)
	1		0.84	0.039	0.038	0.042	0.019	0.015	0.014	0.007
			(3.36	0.161	0.147	0.149	0.094	0.062	0.087	0.037)
	2		0.81	0.037	0.037	0.043	0.017	0.013	0.011	0.007
			(3.14	0.149	0.137	0.146	0.094	0.068	0.071	0.037)
C		night-only χ^2-fitting LST method for cases without night dew (retrieving nighttime ε's)								
	0		0.46	0.020	0.019	0.021	0.011	0.009	0.009	0.012
			(1.75	0.063	0.058	0.064	0.057	0.037	0.034	0.031)
	1		0.44	0.020	0.019	0.021	0.012	0.010	0.011	0.012
			(1.77	0.058	0.059	0.063	0.084	0.039	0.035	0.031)
	2		0.42	0.020	0.019	0.021	0.011	0.009	0.008	0.012
			(1.81	0.068	0.075	0.080	0.092	0.035	0.037	0.031)
D		day-only χ^2-fitting LST method for cases with unknown night dew (retrieving daytime ε's)								
	0	0.74		0.021	0.055	0.059	0.014	0.012	0.013	0.014
		(2.74		0.110	0.304	0.306	0.055	0.047	0.045	0.040)
	1	0.63		0.021	0.028	0.048	0.011	0.009	0.010	0.014
		(3.19		0.111	0.215	0.296	0.046	0.041	0.053	0.040)
	2	0.64		0.021	0.028	0.047	0.011	0.009	0.009	0.014
		(2.69		0.117	0.210	0.277	0.041	0.040	0.043	0.040)
E		day-only χ^2-fitting LST method for cases without night dew (retrieving daytime ε's)								
	0	0.74		0.015	0.066	0.057	0.014	0.012	0.012	0.012
		(2.42		0.059	0.314	0.191	0.074	0.067	0.063	0.031)
	1	0.57		0.017	0.035	0.039	0.009	0.007	0.008	0.012
		(2.42		0.291	0.300	0.265	0.032	0.037	0.064	0.031)
	2	0.56		0.016	0.029	0.040	0.009	0.007	0.007	0.012
		(2.42		0.148	0.287	0.295	0.044	0.032	0.052	0.031)
F		day/night χ^2-fitting LST method for cases with known night dew (retrieving daytime ε's)								
	0	0.74	0.21	0.021	0.055	0.059	0.014	0.012	0.013	0.014
		(2.74	2.09	0.110	0.304	0.306	0.055	0.047	0.045	0.040)
	1	0.63	0.20	0.021	0.028	0.049	0.011	0.009	0.010	0.014
		(3.19	2.09	0.111	0.146	0.296	0.046	0.041	0.053	0.040)
	2	0.63	0.20	0.021	0.030	0.049	0.011	0.009	0.009	0.014
		(2.69	2.09	0.117	0.255	0.277	0.041	0.040	0.043	0.040)
G		day/night χ^2-fitting LST method for cases without night dew (retrieving averaged ε's)								
	0	0.40	0.30	0.014	0.013	0.014	0.008	0.007	0.007	0.012
		(2.02	1.49	0.073	0.065	0.072	0.110	0.033	0.034	0.031)
	1	0.37	0.28	0.013	0.012	0.013	0.007	0.006	0.007	0.012
		(1.75	1.44	0.054	0.051	0.057	0.075	0.029	0.033	0.031)
	2	0.33	0.26	0.011	0.011	0.012	0.006	0.005	0.006	0.012
		(1.77	1.20	0.051	0.055	0.060	0.053	0.027	0.031	0.031)

TABLE IX. Summary of LST values over the test site (38' 31.46'N, 115' 42.74'W) in Railroad Valley, Nevada, during 1:22 and 1:30 PDT on 8/3/95. The size of one MAS pixel is approximately 50m by 50m.

size of area	mean (°C)	stdv (°C)	remarks
12 cm diameter	58.5		by radiometer
5 cm diameter	59.2		by spectrometer at θ_v 20°
1 MAS pixel	59.1		at θ_v 18.75°
3 by 3 MAS pixels	58.9	0.48	
5 by 5 MAS pixels	58.8	0.67	
7 by 7 MAS pixels	58.9	0.76	
9 by 9 MAS pixels	59.0	0.81	
11 by 11 MAS pixels	58.9	0.82	
21 by 21 MAS pixels	58.9	1.21	